Contributions to Mineralogy and Petrology (2022) 177:107
https://doi.org/10.1007/s00410-022-01972-z

ORIGINAL PAPER

Growth of the upper crust in intra-oceanic island arcs by intrusion of basaltic magmas: the case of the Koloula Igneous Complex, Guadalcanal, Solomon Islands (SW Pacific)

Paul Sotiriou[1] · Karsten M. Haase[1] · Kathrin P. Schneider[1] · Anna Grosche[1] · Kristina Noebel[1,2] · Allan R. Chivas[3,4]

Received: 15 April 2022 / Accepted: 27 October 2022 / Published online: 11 November 2022

Abstract

The Pleistocene (2.2–1.5 Ma) Koloula Igneous Complex (KIC) on Guadalcanal in the Solomon island arc consists of a low-K calc-alkaline sequence of ultramafic to felsic plutonic rocks. We present whole-rock major and trace element and Sr–Nd-Pb isotope data, as well as mineral compositions that record the magmatic evolution of the complex. The intrusive sequence is grouped into two cycles, Cycle 1 and 2, comprising gabbroic or dioritic to granodioritic rocks. The major and trace element data of each cycle forms a single calc-alkaline fractional crystallisation trend. The distinct radiogenic isotope and incompatible element compositions of the Cycle 1 and 2 intrusions imply slightly different mantle sources. The KIC formed by shallow (0.1 GPa) fractional crystallisation of mantle-derived Al-rich basaltic parental magmas (6–8 wt.% MgO) that were formed by deeper-level (0.7 GPa) fractionation of olivine and pyroxene from Mg-rich (~ 11 wt.% MgO) primary magmas in the Solomon intra-oceanic island arc. Olivine, clinopyroxene, plagioclase, amphibole, biotite, apatite, and Fe–Ti oxides fractionated from the KIC's high-Al basaltic parental magmas to form calc-alkaline magmas. Liquid line of descent trends calculated using mass balance calculations closely match major element trends observed in the KIC data. The KIC crystallised at shallow, upper crustal depths of ~ 2.0–3.0 km in ~ 20 km-thick island arc crust. This complex is typical of other Cenozoic calc-alkaline ultramafic to felsic plutons in Pacific intra-oceanic island arcs in terms of field relationships, petrology, mineral chemistry and whole-rock geochemistry. Hornblende fractionation played a significant role in the formation of the calc-alkaline felsic plutonic rocks in these Cenozoic arc plutons, causing an enrichment of SiO_2 and light rare earth elements. These plutons represent the fossil magma systems of arc volcanoes; thus, the upper arc crust is probably generated by migration of magmatic centres.

Keywords Solomon Islands · Koloula · Island arcs · Plutonic · Basaltic magmas · Fractional crystallisation

Introduction

The evolution of calc-alkaline magmas from basaltic to rhyolitic compositions is an important process on Earth because andesitic to rhyolitic calc-alkaline rocks comprise large portions of the continental crust and of the upper continental crust in particular (Taylor and McLennan 1985; Rudnick 1995). These magmas typically form at active continental margins with crustal thicknesses of > 30 km; however, seismic studies suggest that intermediate tonalitic rocks also comprise the middle crust of young intra-oceanic island arcs (e.g. Izu–Bonin and Aleutian island arcs) with significantly thinner crust (Suyehiro et al. 1996; Holbrook et al. 1999). The primary magmas in these settings are thought to be generated in the mantle and, therefore, have high-Mg (10–17 wt.% MgO) basaltic compositions (e.g. DeBari 1997;

Communicated by Othmar Müntener.

✉ Paul Sotiriou
paul.sotiriou@fau.de

[1] GeoZentrum Nordbayern, Friedrich-Alexander-Universität (FAU) Erlangen-Nürnberg, Schlossgarten 5, 91054 Erlangen, Germany

[2] Institute for Geochemistry and Petrology, ETH Zürich, Clausiusstrasse 25, 8092 Zürich, Switzerland

[3] School of Earth, Atmospheric and Life Sciences, University of Wollongong, Wollongong, NSW 2522, Australia

[4] Department of Earth Sciences and Sprigg Geobiology Centre, University of Adelaide, Adelaide, SA 5005, Australia

Schmidt and Jagoutz 2017). Intermediate to felsic magmas may form in intra-oceanic island arcs by: (1) shallow fractional crystallisation from basaltic melts (Chivas et al. 1982; Whalen 1985; Müntener and Ulmer 2018); (2) melting of the hydrous lower crust of island arcs (Smith et al. 2003; Saito et al. 2011); (3) lower crustal fractional crystallisation of arc basaltic magmas (Loucks 2021); (4) a combination of deep and shallow (polybaric) fractionation (Almeev et al. 2013; Hamada et al. 2014; Melekhova et al. 2015; Lewis et al. 2021; Marxer et al. 2022); or (5) magma mixing (Eichelberger 1978; Reubi et al. 2003; Reubi and Nicholls 2005; Reubi and Blundy 2009; Ichiyama et al. 2020; Rezeau et al. 2021; Reubi and Müntener 2022).

Models of island arc crust formation suggest a stratification with an ultramafic to mafic lower crust and a felsic upper crust similar to that of the continental crust, and this stratification may form early in the magmatic evolution of island arcs (DeBari 1997; Jagoutz 2014). Whereas the mafic magmas may stagnate in the deep crust and fractionate Mg–Fe-rich minerals, intermediate to felsic melts may ascend into the middle to upper crust (Annen et al. 2006). The accretion of oceanic island arcs to continents is an important process in facilitating the growth of the continental crust (Rudnick 1995; Hawkesworth et al. 2010).

In this contribution, we present new petrologic, geochemical and isotopic data on a suite of ultramafic to felsic plutonic rocks from the Pleistocene Koloula Igneous Complex (KIC) on Guadalcanal in the Solomon island arc. The rocks follow a calc-alkaline fractionation trend, and two intrusive cycles are defined, each defining one liquid line of descent. Most of the early Koloula intrusion cycle consists of gabbroic rocks, representing a mafic intrusion in the upper crust with consecutive fractionation to less voluminous more evolved melts, whereas the later intrusive cycle is more evolved. In this study, we show that the KIC formed by shallow-level fractional crystallisation of mantle-derived basaltic magmas within the Solomon intra-oceanic island arc.

Geological setting

The island of Guadalcanal is part of the Central Province of the Solomon Islands, which are bounded to the north by the tectonically inactive Vitiaz Trench and to the south by the San Cristobal (or South Solomon) Trench where active subduction occurs (Fig. 1). Guadalcanal forms part of the Cretaceous to Quaternary South Solomon MORB terrain (Petterson et al. 1999). The crust beneath Guadalcanal is about 20 km-thick (Segev et al. 2012), and probably consists of Cretaceous mid-ocean ridge basalts (MORBs) and younger island arc rocks (Petterson et al. 1999). Zircon ages support a ~ 96 Ma age for the Cretaceous MORBs and ages of 71 to 33 Ma for the island arc rocks (Tapster et al. 2014). However, xenocrystic zircons with Paleozoic to Archean ages have been found in magmatic rocks from the Oligocene (26–24 Ma) Umasani Complex in western Guadalcanal, suggesting that the Solomon islands may be underlain by continental crust rifted from East Gondwana (Fig. 1; Tapster et al. 2014). There are numerous Pliocene–Holocene volcanic centres in the northwestern part of Guadalcanal and one such volcanic centre at Mbalo near the southeastern coast of the island (Chivas 1978). The nearby island of Savo, located just off the northwestern coast of Guadalcanal, has numerous Pleistocene–Holocene volcanic centres and last erupted in the 1830s and 1840s (Chivas 1977, 1978; Hackman 1978).

The KIC constitutes a low-K calc-alkaline sequence of leucogabbros, gabbros, pyroxenites, diorites, quartz diorites, tonalites, granodiorites, trondhjemites, and aplites (Chivas 1977, 1978; Chivas and McDougall 1978; Chivas et al. 1982; Tapster et al. 2016). This plutonic complex formed by more than 30 intrusions that have been grouped into 2 cycles (Cycle 1 and 2), the first of which occurred in the early Pleistocene (2.2 Ma; Gelasian age) in the form of gabbroic and ultramafic cumulates that evolved to diorite, quartz diorite, and granodiorite (Fig. 2; Chivas 1977, 1978; Chivas and McDougall 1978; Tapster et al. 2016). The second cycle consists of mid-Pleistocene (1.7–1.45 Ma; Calabrian age) diorite and tonalite bodies comprising the concentrically zoned Inamumu Pluton (Fig. 2), which was intruded by aplite and trondhjemite dykes and two porphyritic tonalites (Fig. 2; Chivas and McDougall 1978; Tapster et al. 2016). The emplacement and crystallisation ages of the KIC were previously determined by K–Ar dating to be between 4.5 and 1.5 Ma (Chivas and McDougall, 1978). Rapid uplift (> 2 km) since the early Pleistocene and significant erosion has exposed the KIC (Chivas et al. 1982). Both Cycles 1 and 2 are intrusive into the spatially associated Early Miocene Suta Volcanics, which comprise pillow and massive lavas of basaltic to andesitic composition (Chivas 1977, 1978).

The KIC contains a porphyry Cu mineral prospect, with an estimated 50 Mt of ore at a low grade of 0.17% Cu (Holm et al. 2019; Keith et al. 2022). This mineralisation formed ~ 250 ka after the initial intrusion of the Cycle 2 rocks, with the so-called A and B systems of hydrothermal alteration forming at 1.46 Ma (Chivas and McDougall 1978). Late magmatic activity is indicated by the emplacement of post-mineralisation andesitic dykes (Chivas and McDougall 1978). The constant Sr isotopic compositions ($^{87}Sr/^{86}Sr = 0.70363–0.70378$) of rocks with variable SiO_2 and MgO contents were interpreted by Chivas et al. (1982) to reflect a liquid line of descent for the entire KIC.

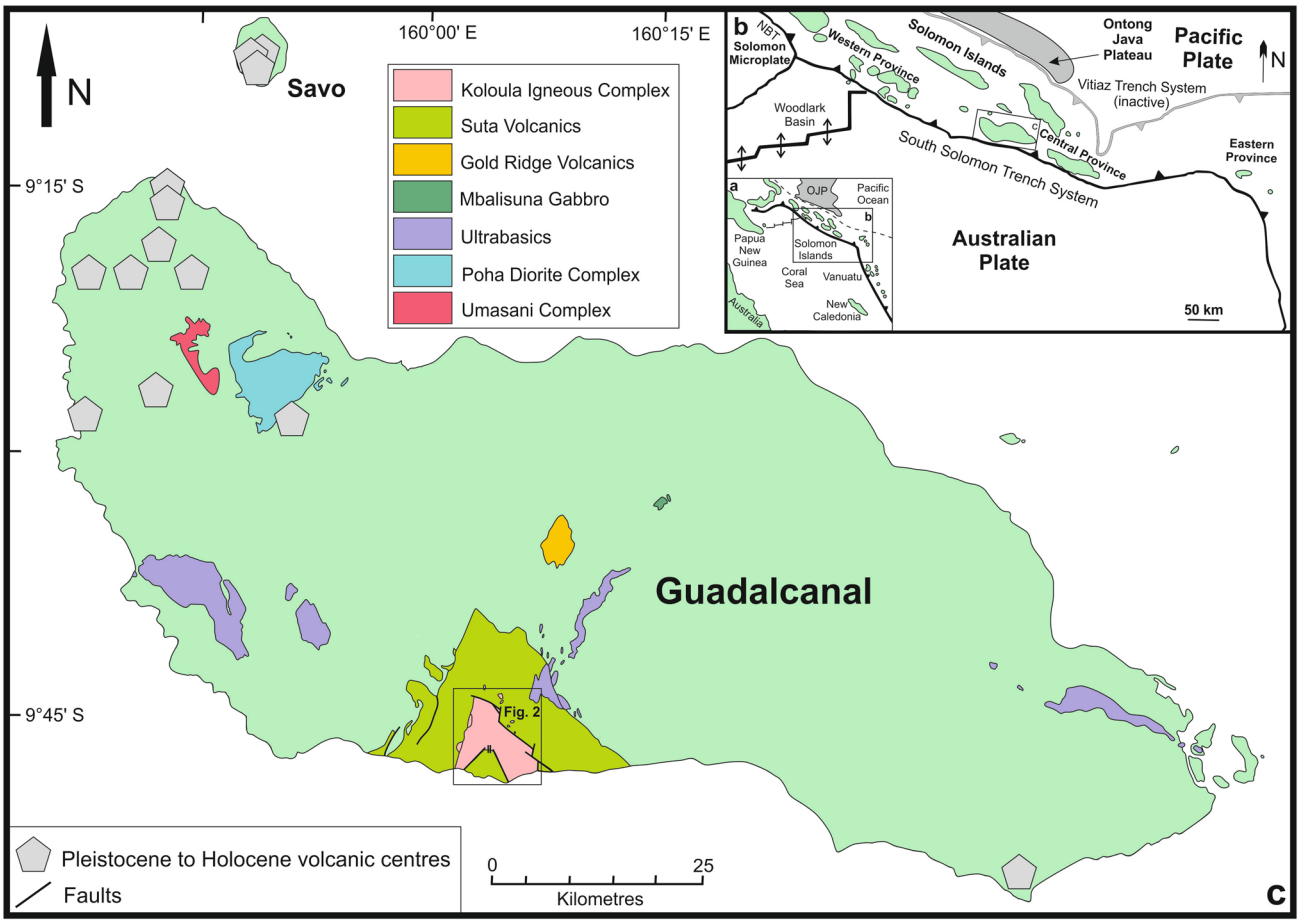

Fig. 1 **a** Inset map showing the location and setting of the Solomon island arc in the southwestern Pacific region (modified after Schuth et al. 2009). OJP: Ontong Java Plateau. **b** Inset map showing the location of Guadalcanal in the Solomon Island arc (modified after Schuth et al. 2009). NBT: New Britain Trench. **c** Geological map of Guadalcanal (modified after Chivas 1978 and Hackman 1978)

Analytical methods

Sampling and sample preparation

Samples representing the variable lithologies of both intrusive cycles were collected during mapping field work on Guadalcanal in 1972–1975 (Chivas 1977). Some samples were previously analysed (Chivas 1977) and share the same field sample numbers. For the more recent analyses, rock powders were prepared afresh from original remnant hand specimens. Unaltered pieces were cut with a rock saw for geochemical analysis and thin section preparation. The whole-rock pieces were washed in an ultrasonic bath with deionised water and dried for 12 h at 60 °C. The clean geochemistry pieces were crushed using a hydraulic press and reduced to powder in an agate ball mill. The powders were dried for 12 h at 104 °C prior to fusion for major element analysis.

Mineral analyses

Thin sections of 20 samples were studied under the microscope, and mineral analyses were measured using a JEOL JXA 8200 Superprobe electron microprobe at the GeoZentrum Nordbayern (GZN), Friedrich-Alexander Universität Erlangen-Nürnberg, Erlangen, Germany, following methods and using standards described in Schaarschmidt et al. (2021). Plagioclase, hornblende, pyroxene, biotite and apatite compositions were measured with a 3 µm electron beam diameter at a 15 kV acceleration voltage and a beam current of 15 nA. Olivine was measured at an optimal 20 kV acceleration voltage and with a 1 µm beam diameter and a current of 20 nA. The detection limit was < 50 µg/g for SiO_2, CaO, K_2O, Al_2O_3, Na_2O, MgO, P_2O_5, Cr_2O_3, Cl, SrO and SO_3, and < 100 µg/g for FeO_{tot}, MnO, NiO and TiO_2. All measured mineral data are presented in Table S1 (T1) of Electronic Supplementary Material (S) 1. The Mg# values of clinopyroxene, orthopyroxene, amphibole, and

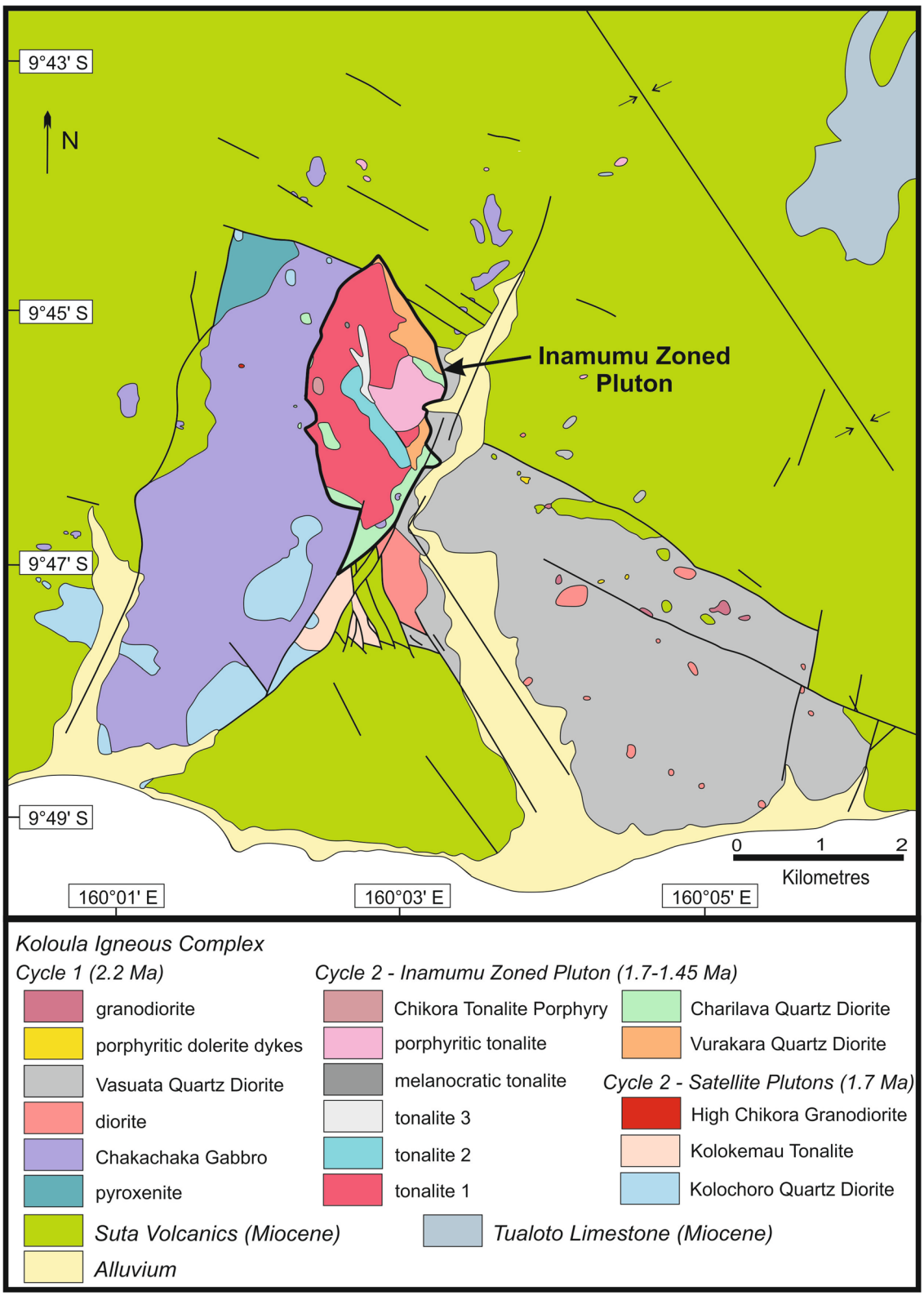

Fig. 2 Geological map of the KIC and the spatially associated Suta Volcanics (modified after Chivas 1978 and Hackman 1978). The position of the elliptical Cycle 2 Inamumu Zoned Pluton (IZP) is outlined with a bold line. Other Cycle 2 satellite plutons, of the same initial age (1.7 Ma), comprise the Kolochoro Quartz Diorite, Kolokemau Tonalite and the High Chikora Granodiorite, mostly crop out to the south and west of the IZP. The other rock units, with generally larger outcrop areas, comprise the Cycle 1 (earlier) igneous rocks.

biotite were calculated using the formula Mg# = (MgO/40.3/((MgO/40.3) + (FeO_{tot}/71.84))) * 100. Similarly, the Fo contents of olivine were obtained using the formula Fo = (MgO/40.3/((MgO/40.3) + (FeO_{tot}/71.84))) * 100. The An contents of plagioclase were determined utilising the formula An = (CaO/56.1/((CaO/56.1) + (Na_2O/31) + (K_2O/48))) * 100. The amphibole geobarometer of Ridolfi et al. (2010) was applied to amphibole analyses from the KIC.

Whole-rock element analyses

The major element concentrations of 42 whole-rock samples were analysed using a Spectro XEPOS He X-ray fluorescence spectrometer at the GZN. Further details of the analytical techniques are provided in Freund et al. (2013). The accuracy and precision of the measurements were determined by multiple measurements of the international rock standards BE-N, BR, AC-E and GA (Table S2). The accuracy was generally better than ~ 3% (2σ), except for P_2O_5, which was better than 7.5%. The precision was better than 0.1–0.2%. Trace element analyses of 42 samples from the KIC were determined at the GZN on a Thermo Fisher Scientific XSeries 2 Quadrupole Inductively Coupled Plasma Mass Spectrometer (ICP-MS) connected to an Aridus 2 membrane desolvating sample introduction system. Major and trace element whole-rock geochemical data from the KIC are presented in Table S3. The Eu/Eu* and Ti/Ti* anomalies in Table S3 were calculated using the methods set out in Taylor and McLennan (1985). The normalised ratios in Table S3 were calculated based on the chondrite values in Sun and McDonough (1989).

Whole-rock Sr, Nd and Pb isotope analyses

Strontium, Nd and Pb isotope analyses on 17 samples were performed at the GZN. Strontium and Nd isotopes were analysed using a Thermo-Fisher Triton thermal ionisation mass spectrometer (TIMS) in static mode following the chemical and analytical procedures outlined in Haase et al. (2017). Strontium isotope measurements were corrected for mass fractionation assuming $^{88}Sr/^{86}Sr = 0.1194$, where mass 85 was monitored to correct for the contribution of ^{87}Rb to ^{87}Sr. Neodymium isotope data were corrected for mass fractionation using $^{146}Nd/^{144}Nd = 0.7219$. Samarium interferences on masses 144, 148, 150 were corrected by measuring ^{147}Sm, but the correction was insignificant for all samples. The maximum internal uncertainty was 0.000007 for $^{87}Sr/^{86}Sr$ and 0.000005 for $^{143}Nd/^{144}Nd$ (2σ). During the measurements, the NBS987 standard yielded $^{87}Sr/^{86}Sr = 0.710278$ (2σ, $n = 6$) and the Erlangen Nd standard gave $^{143}Nd/^{144}Nd = 0.511534$ (2σ, $n = 4$), which corresponds to a value of 0.511850 for the La Jolla Nd isotope standard determined at the GZN.

Lead isotope measurements were carried out on a Thermo-Fisher Neptune MC–ICP-MS in static mode using a $^{207}Pb/^{204}Pb$ double spike to correct for instrumental mass fractionation. Details of the Pb isotope procedures and analytical techniques are discussed by Woelki et al. (2018). The Pb fraction was diluted with 2% HNO_3 to a concentration of approximately 20 ppb. One part of this solution was spiked to obtain a $^{208}Pb/^{204}Pb$ ratio of ~ 1. The double spike, with a $^{207}Pb/^{204}Pb$ ratio of 0.5, was calibrated against a solution of the NBS982 equal atom Pb standard. Spiked and unspiked sample solutions were introduced into the plasma via a Cetac Aridus desolvating nebuliser, and measured in static mode. Interference of ^{204}Hg on mass 204 was corrected by monitoring ^{202}Hg. An exponential fractionation correction was applied offline using the iterative method of Compston and Oversby (1969); the correction was typically 4.5‰ per amu.

The internal uncertainty was 0.0003, 0.0003 and 0.0008 (2σ) for $^{206}Pb/^{204}Pb$, $^{207}Pb/^{204}Pb$ and $^{208}Pb/^{204}Pb$, respectively. Measurements of the NBS981 Pb isotope standard (measured as an unknown) over the course of this study gave $^{206}Pb/^{204}Pb$, $^{207}Pb/^{204}Pb$, $^{208}Pb/^{204}Pb$ ratios of 16.9405 ± 0.0021, 15.4980 ± 0.0018 and 36.7199 ± 0.0040, respectively (2σ, $n = 13$). Lead data in Table S4 have been normalised to values of 16.9410, 15.4993 and 36.7244 for the NBS981 Pb isotope standard. Analyses of the aforementioned isotope standards are presented in Table S2. Radiogenic Sr, Nd and Pb isotope data from the KIC are shown in Table S4.

Results

Petrography and mineral composition of the plutonic rocks

The rocks of the KIC range from coarse-grained cumulates to fine-grained dykes, and include pyroxenites, gabbros, leucogabbros, anorthositic segregations, diorites, quartz diorites, tonalites, granodiorites, trondhjemites, and aplites. Mg-rich olivine (Fo_{75-82}) occurs in the pyroxenites of Cycle 1 (T1). Plagioclase is abundant in most rock types and ranges in composition from An_2 to An_{99} (Fig. 3). This mineral is partially altered to zoisite, epidote and albite (i.e. undergone saussuritisation). Clinopyroxene (Mg# = 68–90) is abundant but is partially altered to actinolite. Magnesium-rich clinopyroxene (Mg# = 75–90) mostly occurs in the pyroxenites and gabbros of Cycle 1; however, Mg-rich clinopyroxene (Mg# = 75–79) is also found in the Cycle 2 Kolochoro Quartz Diorite. Orthopyroxene (Mg# = 66–84) is rare and is surrounded by hornblende reaction rims. Primary hornblende (Mg# = 47–88) occurs in approximately half of the samples and is partially altered to actinolite. Hornblende and clinopyroxene occur as oikocrysts, which envelop small

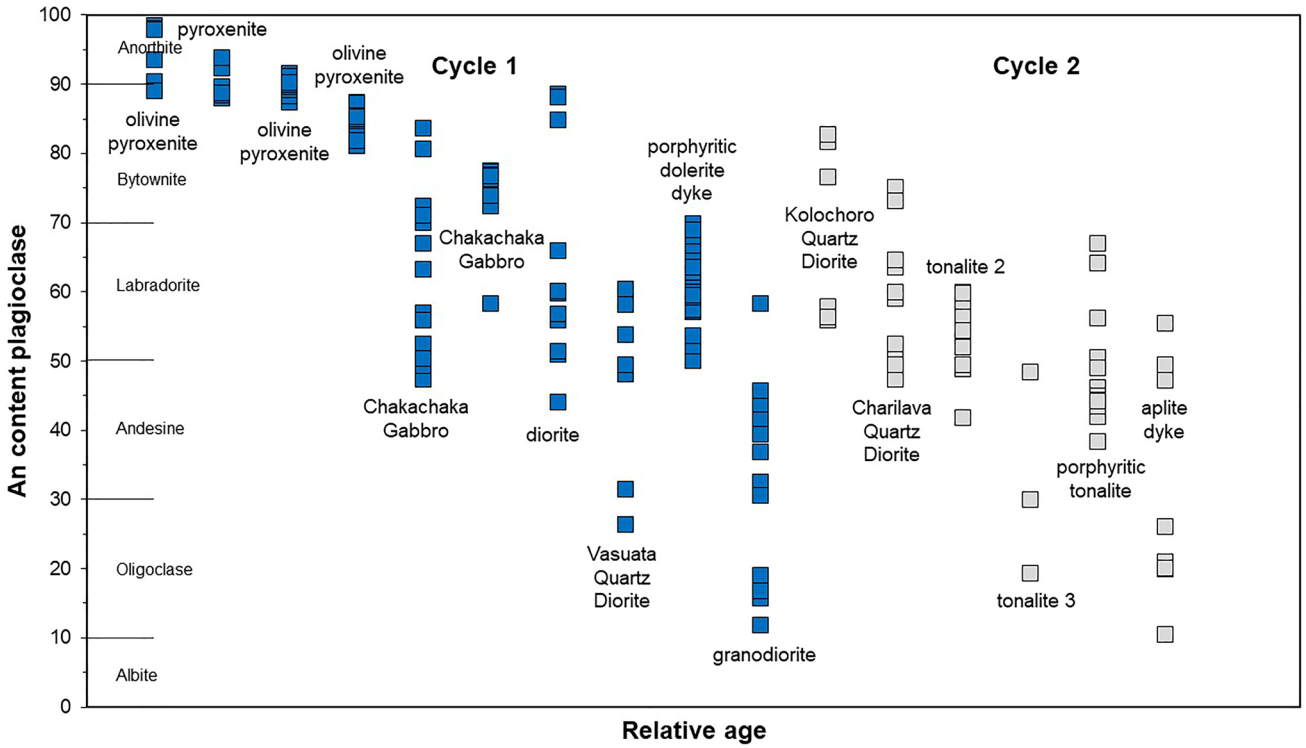

Fig. 3 Plagioclase anorthite content versus relative age diagram for Cycles 1 and 2 of the KIC. The relative ages of the different phases of the KIC are based on field relationships

plagioclase crystals and have serrated grain boundaries with cumulus plagioclase. Biotite (Mg# = 57–67) is present in approximately half of the samples. Potassium feldspar occurs in the diorites, quartz diorites, tonalites, granodiorites and aplites and forms 5–60% of these lithologies. Apatite occurs in the tonalites and granodiorites and comprises up to 5% of these lithologies. Oxides (magnetite and ilmenite) comprise 1–4% of the lithologies present in the KIC. Quartz comprises 5–40% of the diorites, quartz diorites, tonalites, granodiorites, and aplites.

There is a progressive decrease in the anorthite content of plagioclase from the Cycle 1 to Cycle 2 intrusions of the KIC (Fig. 3; Table S1). The anorthite contents of plagioclase decrease from Cycle 1 (An_{12-98}) to Cycle 2 (An_{10-82}). Moreover, there is a decrease in the anorthite content of plagioclase within both cycles over time (Fig. 3). The higher average An contents of plagioclase from the Cycle 1 intrusions are attributed to the greater occurrence of cumulate rocks within this cycle and a paucity of similar lithologies in the Cycle 2 intrusions. Plagioclase crystals from Cycle 1 lithologies younger than the Chakachaka Gabbro have overlapping An contents with those from the Cycle 2 intrusions. The most evolved lithologies in the Cycle 1 intrusions have plagioclase crystals with lower An contents than the Cycle 2 quartz diorites and tonalites.

It should be pointed out that the plagioclase An content variations in the Cycle 1 and 2 lithologies were from the analysis of only a few plagioclase grains per sample and that some of these grains exhibit oscillatory zoning. Profiles across plagioclase grains reveal either constant or decreasing An contents from core to rim in the majority of analysed samples (e.g. from An_{75} to An_{47} in the Charilava Quartz Diorite). However, some zoned plagioclase grains from the olivine pyroxenites (Cycle 1) show slightly increasing An contents during crystal growth (e.g. from An_{82} to An_{87}). Normal zoning of plagioclase grains generally supports a magma evolution dominated by crystallisation without significant assimilation or magma mixing. Yet, weak inverse zoning of plagioclase in the pyroxenites indicates that recharge of mafic magmas affected the Koloula magmatic system during its early stages. The outlying plagioclase An contents (e.g. the high-An contents in the Cycle 1 diorite or the low-An contents in the Cycle 1 granodiorite) in some of the samples may be indicative of other processes. For instance, the high-An contents of plagioclase in the Cycle 1 diorite may represent high-An cores that crystallised at an earlier magmatic stage at deeper crustal levels or xenocrystals entrained from pre-existing magmatic lithologies. The low-An contents of plagioclase in the Cycle 1 granodiorite could be attributed to alteration.

Major element variations

The samples from the KIC vary from ultramafic to felsic in composition with a range from 0.1 to 20 wt.% MgO and 43 to 78 wt.% SiO_2 (Fig. 4; Table S3 and Table S5). The Koloula plutonic samples show similar major element trends to volcanic rocks from the Solomon arc (Figs. 1 and 4; Tables S3-S6). A key feature of the Koloula plutonic samples is that they have decreasing CaO, MgO and FeO^T contents with increasing SiO_2 (Fig. 4; Table S3 and Table S5; König & Schuth, 2011). The MgO contents of the Koloula plutonic samples range from 20 to 6 wt.% at 46–50 wt.% SiO_2 before decreasing from 6 wt.% MgO at 50 wt.% SiO_2 to 0 wt.% MgO at 78 wt.% SiO_2 (Fig. 4a). The TiO_2 contents of the Koloula plutonic rocks vary between 0.15 and 1.0 wt.% in the mafic plutonic rocks (Table S3 and Table S5). The KIC plutonic rocks with > 52 wt.% SiO_2 show decreasing TiO_2 contents. The Al_2O_3 contents decrease slightly from 18 to 17 wt.% between 49 and 62 wt.% SiO_2 and then decrease more steeply towards higher SiO_2 contents (Fig. 4b). The FeO^T and CaO contents in the mafic rocks are ~ 10 and 12 wt.%, respectively, and decrease to 0.7 and 0.8 wt.%, respectively, in the aplites (Fig. 4c, d). The Na_2O contents increase from 0.4 to 5.0 wt.% with increasing SiO_2 (Fig. 4e). The K_2O contents increase from 0.2 wt.% in the mafic rocks to 1.8 wt.% in the tonalites, whereas two aplites contain 5.5 and 7.2 wt.% K_2O (Table S3 and Table S5). The P_2O_5 concentrations are < 0.1 wt.% in the mafic rocks but increase to 0.25 wt.% in rocks with ~ 53–56 wt.% SiO_2 before decreasing steeply to 0.08 wt.% in the aplites (Fig. 4f).

Trace element variations

The normal mid-ocean ridge basalt (N-MORB)-normalised trace element patterns of the KIC rocks exhibit negative Nb and positive Pb anomalies, whilst the Cycle 1 and 2 intrusions are distinctive (Fig. 5). The Cycle 2 intrusions have more evolved trace element patterns displaying higher incompatible element concentrations than the Cycle 1 intrusions. The Cycle 1 and 2 intrusions have trace element patterns that overlap with those of lavas from the Solomon arc (Fig. 5; König and Schuth 2011). Some Cycle 2 samples have higher Th, U, MREE and HREE normalised abundances than the Solomon Islands lavas, whereas other Cycle 2 samples have lower MREE and HREE normalised abundances than these lavas. One Cycle 1 sample has higher MREE and HREE normalised abundances than the Solomon arc lavas.

The trace element ratios of lavas from the Solomon arc mostly overlap with those of the KIC (Fig. 6). The $(Dy/Yb)_N$ ratios in Cycles 1 and 2 are almost constant at ~ 1 (Fig. 6a). There are higher $(Ce/Yb)_N$ and $(La/Sm)_N$ ratios in samples from Cycle 2 than those from Cycle 1 (Fig. 6b, d). Cycle 1 and 2 samples have constant Eu/Eu* anomaly ratios of ~ 1 (Fig. 6c). Moreover, the Ba/La ratios of Cycle 1 intrusions vary between 20 and 40; however, most Cycle 2 samples with > 60 wt.% SiO_2 have higher Ba/La ratios of 40–60 (Fig. 6e). The Koloula plutonic samples have near-constant Nb/La ratios (0.1–0.3) for a given SiO_2 content; however, the Cycle 2 intrusions generally have lower Nb/La ratios than the Cycle 1 intrusions (Fig. 6f).

Isotope variations of the Koloula plutonic rocks

As pointed out by Chivas et al. (1982), the Koloula plutonic rocks show a narrow range of radiogenic isotope compositions and we find near-constant Sr, Nd and Pb isotope ratios for the entire ultramafic to felsic compositional range (Figs. 7 and 8). Samples from Cycle 2 have overlapping $^{143}Nd/^{144}Nd$ and $^{87}Sr/^{86}Sr$ isotope ratios to those from Cycle 1 (Fig. 7). Cycle 1 and 2 intrusions have distinct Pb radiogenic isotope compositions (Fig. 8). The $^{206}Pb/^{204}Pb$ isotope ratios of samples from Cycle 2 are less radiogenic than those of the Cycle 1 samples when plotted against $^{207}Pb/^{204}Pb$, $^{208}Pb/^{204}Pb$, $^{87}Sr/^{86}Sr$ and $^{143}Nd/^{144}Nd$ (Fig. 8).

Discussion

Estimation of the emplacement depth of the KIC

Fluid inclusion evidence from the porphyry Cu mineralisation within the KIC has been used to estimate the lithostatic load (~ 3.3 km) of the complex (Chivas and Wilkins 1977). This initial depth of emplacement estimate (~ 3.3 km) of the IZP (Cycle 2) was based on fluid-inclusion geobarometric determinations using the phase equilibria of Sourirajan and Kennedy (1962) and using a rock density of 2.6 g/cm^{-3}. Subsequent experimental data from Bodnar et al. (1985), particularly for the relevant temperature range of 500–700 °C, permit a re-evaluation of this depth of emplacement estimate, wherein the calculated parameters, with assigned homogenisation errors of ± 10–15 °C, provide trapping pressures of 525–630 bar (0.053–0.065 GPa) which, using a rock density of 2.6 g/cm^{-3}, translates to a lithostatic load of 2.0–2.5 ± 0.25 km. Roedder and Bodnar (1980) caution that such calculations may represent minimum pressures for such systems if, as in this case, the inclusions trapped a highly saline albeit unsaturated solution. This depth estimate pertains only to the IZP and, by extension, given they are of the same age, the Cycle 2 satellite plutons. The older Cycle 1 lithologies are assumed to have intruded at a slightly greater depth (~ 3 km), as they can be expected to have been semi-continuously uplifted since their emplacement. The high anorthite contents of plagioclase (up to An_{99}) from the KIC suggest that its parental magmas likely formed by partial

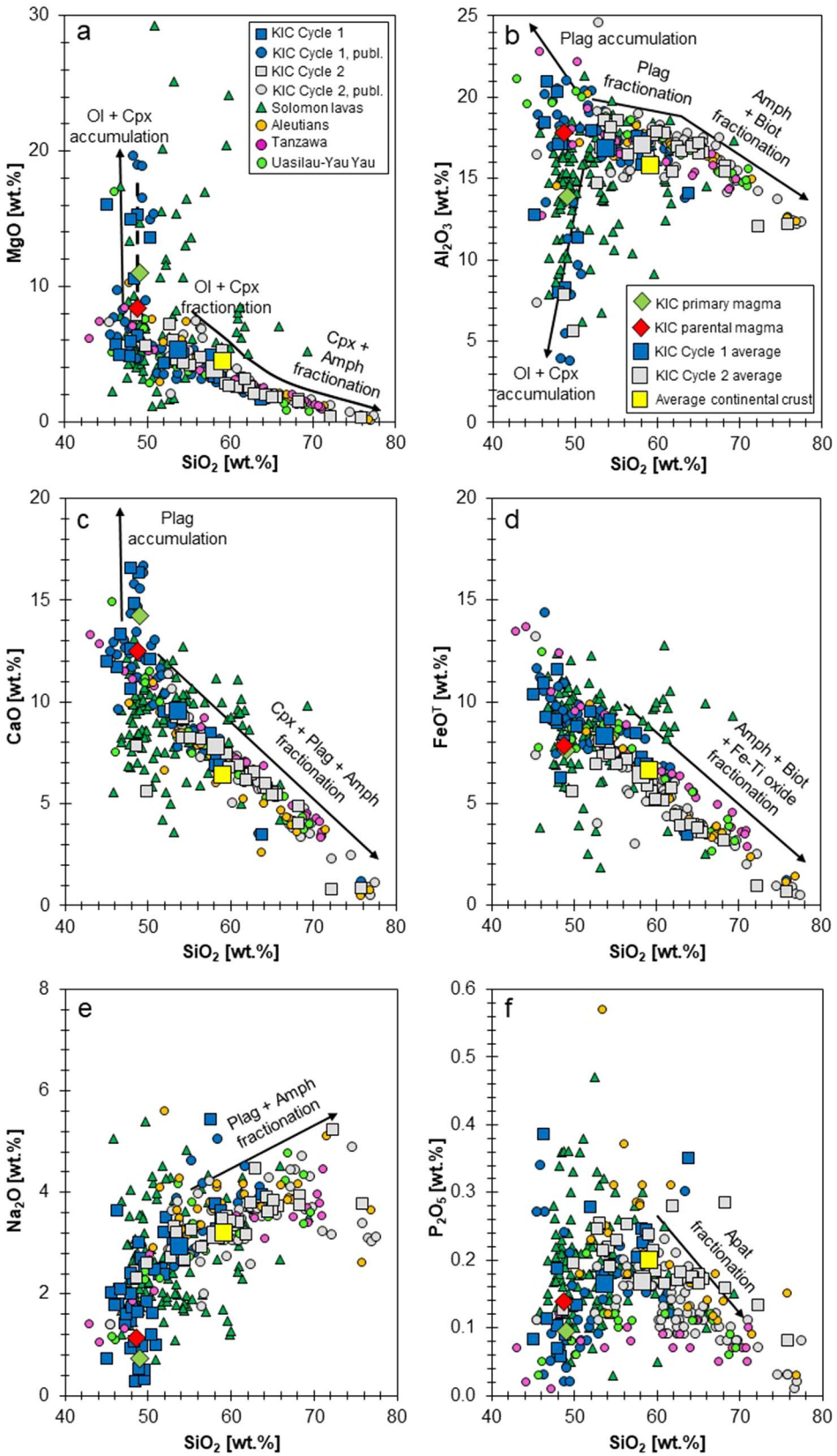
a
KIC Cycle 1
KIC Cycle 1, publ.
KIC Cycle 2
KIC Cycle 2, publ.
Solomon lavas
Aleutians
Tanzawa
Uasilau-Yau Yau
Ol + Cpx accumulation
Ol + Cpx fractionation
Cpx + Amph fractionation
MgO [wt.%]
SiO2 [wt.%]
b
Plag accumulation
Plag fractionation
Amph + Biot fractionation
Ol + Cpx accumulation
KIC primary magma
KIC parental magma
KIC Cycle 1 average
KIC Cycle 2 average
Average continental crust
Al2O3 [wt.%]
SiO2 [wt.%]
c
Plag accumulation
Cpx + Plag + Amph fractionation
CaO [wt.%]
SiO2 [wt.%]
d
Amph + Biot + Fe-Ti oxide fractionation
FeOT [wt.%]
SiO2 [wt.%]
e
Plag + Amph fractionation
Na2O [wt.%]
SiO2 [wt.%]
f
Apat fractionation
P2O5 [wt.%]
SiO2 [wt.%]

◂**Fig. 4** Major element variation diagrams for the KIC. **a** MgO (wt.%), **b** Al_2O_3, **c** CaO (wt.%), **d** FeO^T (wt.%), **e** Na_2O (wt.%) and **f** P_2O_5 (wt.%) are plotted against SiO_2 (wt.%). These diagrams demonstrate that the MgO, CaO and FeO^T contents of the KIC decrease with increasing SiO_2, whereas the Na_2O contents increase with increasing SiO_2. The Al_2O_3 contents of the KIC gently decrease between ~ 49 and ~ 62 wt.% SiO_2 before decreasing more steeply with increasing SiO_2. The P_2O_5 contents of the KIC increase up to 56 wt.% SiO_2 before decreasing due to apatite fractionation. The direction of fractionation and the involved fractionating minerals are highlighted by the fractionation arrows (Ol: olivine; Cpx: clinopyroxene; Plag; plagioclase; Apat: apatite; Amph: amphibole; Biot: biotite). The crystallisation of cumulate lithologies and their constituent cumulate minerals (e.g. olivine, clinopyroxene, plagioclase) are indicated by the accumulation trend arrows. Published data for the KIC are from Chivas (1977), Chivas et al. (1982) and Tapster et al. (2016). Data shown for the Solomon arc lavas are from Chivas (1977), Schuth et al. (2004, 2009); König et al. (2007), and König and Schuth (2011). The average compositions of Cycle 1 and 2 are indicated by the enlarged navy-blue and grey squares, respectively. These average compositions were determined by averaging the compositions of the Cycle 1 and Cycle 2 samples. The modelled composition (Table S7) of the primary magma to the KIC is shown by the green diamonds. The modelled composition (Table S7) of the parental magma to the KIC is shown by the red diamonds. The dashed line in **a** represents an olivine control line. Cenozoic arc pluton data sources: Tanzawa Plutonic Complex (Japan)—Kawate and Arima (1998) and Suzuki et al. (2015); Uasilau-Yau Yau Intrusive Complex (Papua New Guinea)—Whalen (1985); Hidden Bay and Kagalaska plutons (Alaska, USA)—Kay et al. (2019); Yavuna, Colo and Momi plutons (Fiji)—Marien et al. (2022). The large yellow squares represent the composition of average continental crust from Rudnick (1995)

melting of a hydrous sub-arc mantle source and crystallised at a shallow depth (e.g. Sisson and Grove 1993a, b; Takagi et al. 2005). Moreover, amphibole barometry after Ridolfi et al. (2010) suggests crystallisation pressures of between 0.04 and 0.1 GPa (2.7–4.0 km) for most of the analysed Cycle 1 and 2 phases. This is in good agreement with the formation depth of the porphyry Cu mineralisation in the KIC (Chivas and Wilkins 1977) and implies near-constant intrusion depths for both cycles. Higher estimated pressures (0.14–0.24 GPa) for amphibole from the Kolochoro Quartz Diorite (Cycle 2) may suggest that amphibole in the KIC started crystallising at a greater depth and implies temporal magma stagnation at depths of ca. 5–9 km. Finally, the emplacement of this complex into the pillow-bearing basaltic to andesitic lavas of the Suta Volcanics indicates that it formed in shallow oceanic arc crust (Chivas 1977, 1978).

Constraints on the compositions of the KIC's primary and parental magmas

The Cycle 1 intrusions from the KIC have a basaltic composition similar to the mafic lavas from the Solomon island arc (Fig. 4). This implies that the plutonic rocks of the KIC largely reflect melt compositions rather than cumulates, except for the pyroxenites, gabbros, leucogabbros and anorthositic segregations (Fig. 4; Table S3 and Table S5). The Mg-rich (> 10 wt.% MgO) plutonic rocks in the KIC likely represent cumulates rather than melt compositions on account of their coarse-grained cumulate textures (Fig. 4). There are no known cross-cutting high-Mg dykes within the KIC that are representative of the high-Mg primary magmas to this complex. The Fo contents (75–82) of olivine from the KIC are not in equilibrium with the Mg# of Mg-rich lavas from the Solomon (Mg#=72-82) arc (Table S6) due to fractionation of olivine and clinopyroxene from the KIC's parental magma. To test whether the KIC had Mg-rich primary magmas, the composition of the KIC's primary magma was modelled using the reverse crystallisation tab in the Petrolog3 software of Danyushevsky and Plechov (2011). The starting composition was Kolochoro Quartz Diorite sample A.498, which was selected because it represents the most primitive composition in the KIC that can still be considered as a melt. Fractionation of this primary magma was assumed to occur at a pressure of 0.7 GPa at the base (~ 20 km) of the Solomon island arc crust (Furumoto et al. 1970; Segev et al. 2012; Electronic Supplementary Material (S) 2). A temperature of 1280 °C and an oxygen fugacity of QFM + 2.2 were assumed on the basis of temperature and fO_2 values reported in Rohrbach et al. (2005) for picrites from the nearby New Georgia Group to the west of Guadalcanal. A starting H_2O content of 1 wt.% was used based on the H_2O content of sample A.498. Olivine and clinopyroxene mineral-melt models from Ariskin et al. (1987) were used in the modelling due to these models being applicable to upper to lower crustal crystallisation pressures, island arc settings and basaltic compositions. This modelling indicates that the primary magmas to the KIC were Mg-rich (ca. 11 wt.% MgO) and basaltic in composition (indicated by the green diamonds in Fig. 4; see Tables S7 and S2 for details on the modelling input parameters). These Mg-rich primary magmas (SiO_2 = 49.0 wt.%, Al_2O_3 = 13.9 wt.%, MgO = 11.0 wt.%, CaO = 14.2 wt.%; T7) have lower MgO contents than primary arc magmas from the Sunda, Aleutian, Honshu, New Hebrides and Lesser Antilles arcs (Table S7). However, the KIC's primary magmas were likely generated by hydrous melting of depleted mantle sources in subduction zones (Figs. 4 and 5; Tables S3-S5; Pichavant et al. 2002; König and Schuth 2011; Schmidt and Jagoutz 2017; Müntener and Ulmer 2018).

The modelled primary magma of the KIC (the green diamond in Fig. 4) was used as a starting composition to test whether a high-Al basaltic magma can be generated by fractionation of olivine and pyroxene at depth (e.g. Kay et al. 2019). The composition of the KIC's parental magma was determined using the crystallisation tab in the Petrolog3 software. The starting H_2O content was assumed to be 0.74 wt.% and was derived from the modelled H_2O content of the KIC's primary magma (Table S7). This assumption was supported by the application of

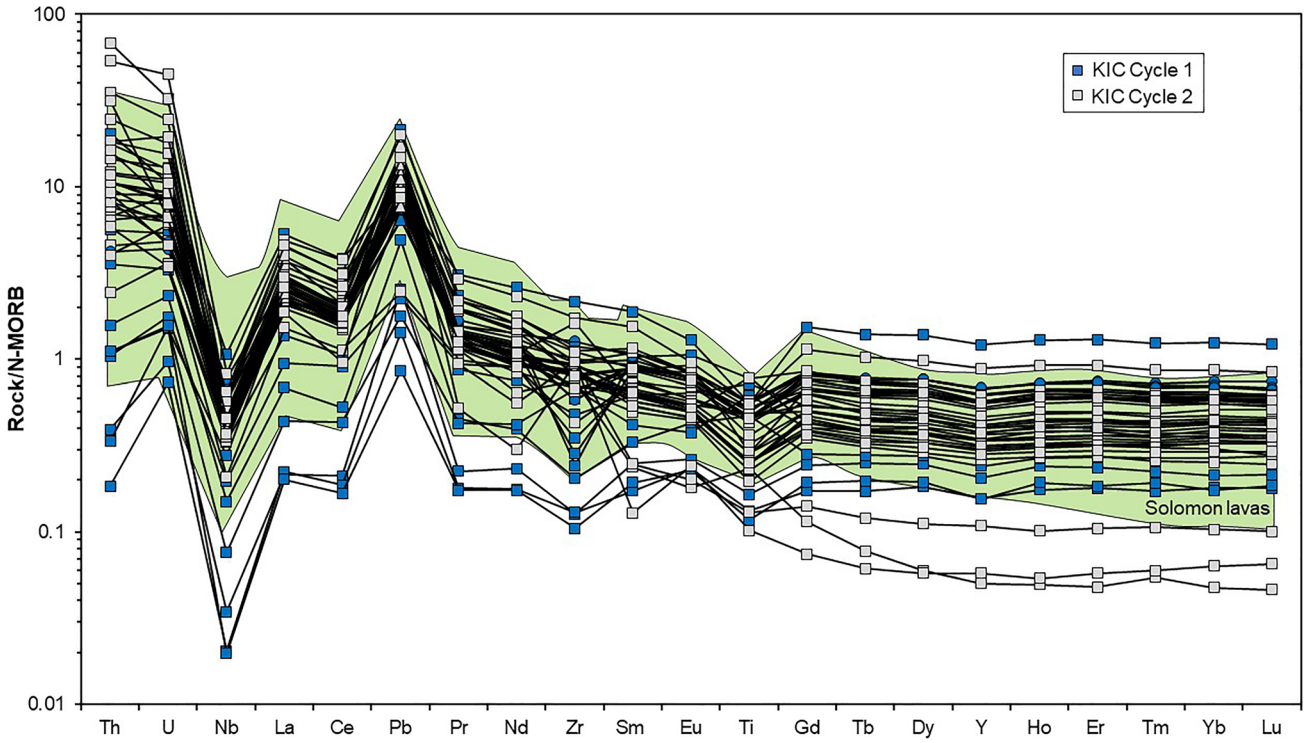

Fig. 5 N-MORB-normalised trace element diagram for Cycle 1 and Cycle 2 of the KIC. This diagram shows that the Cycle 2 intrusions have more evolved N-MORB-normalised trace element abundances than the Cycle 1 intrusions. The ranges of N-MORB-normalised trace element patterns for lavas from the Solomon arc are shown in the background (Data sources: König and Schuth 2011). The N-MORB normalisation values are from Sun and McDonough (1989)

the Putirka (2008) plagioclase hygrometer, which when applied to whole-rock and plagioclase compositions indicates that the KIC parental magma had a H_2O content of ~ 0.6 wt.%. An oxygen fugacity value of Ni-NiO + 1.4 was used during the modelling calculations and was also obtained during the primary magma composition modelling (see S2). It is assumed that fractional crystallisation occurred at a pressure of 0.7 GPa at the base (~ 20 km) of the Solomon intra-oceanic island arc (Furumoto et al. 1970; Segev et al. 2012). The modelling was stopped at 100% of fractionation and the fractionation percentages for olivine and clinopyroxene were set at 35% each after being increased from 20% each based on Kay et al. (2019). The selection of olivine and clinopyroxene fractionation percentages was also guided by the compositions of the KIC's mafic plutonic lithologies. The resultant modelled basaltic parental magma to the KIC resembles a high-Al basalt (SiO_2 = 48.7 wt.%, Al_2O_3 = 16.7 wt.%, MgO = 8.4 wt.%, CaO = 12.5 wt.%; Table S7). This modelled parental magma composition indicates that the MgO-rich primary magmas to the KIC underwent olivine and pyroxene fractionation (e.g. Kay et al. 2019) at the base of the Solomon arc crust (ca. 20 km depth) to form the high-Al basaltic parental magmas to the KIC.

An appraisal of a fractional crystallisation origin for the KIC

Chivas et al. (1982) proposed that the KIC formed by fractional crystallisation of mantle-derived basaltic magmas. This model is supported by linear trends exhibited by the KIC data in major element variation diagrams (Fig. 4). To test whether the KIC formed by fractional crystallisation, the mass balance equation in Jagoutz (2010) was used to calculate the compositions of melts that was formed by fractional crystallisation (see Table S7 and S2 for further details). This mass balance equation was applied to a starting melt composition (the modelled high-Al basaltic parental magma to the KIC) and averaged cumulate compositions from the KIC. Melt compositions were calculated for ten successive fractionation steps by successively changing the fractionating compositions from gabbro to quartz diorite to tonalite to aplite. It should be noted here that Jagoutz (2010) used lithologies ranging from dunites to tonalites as fractionating cumulate compositions, the more evolved of

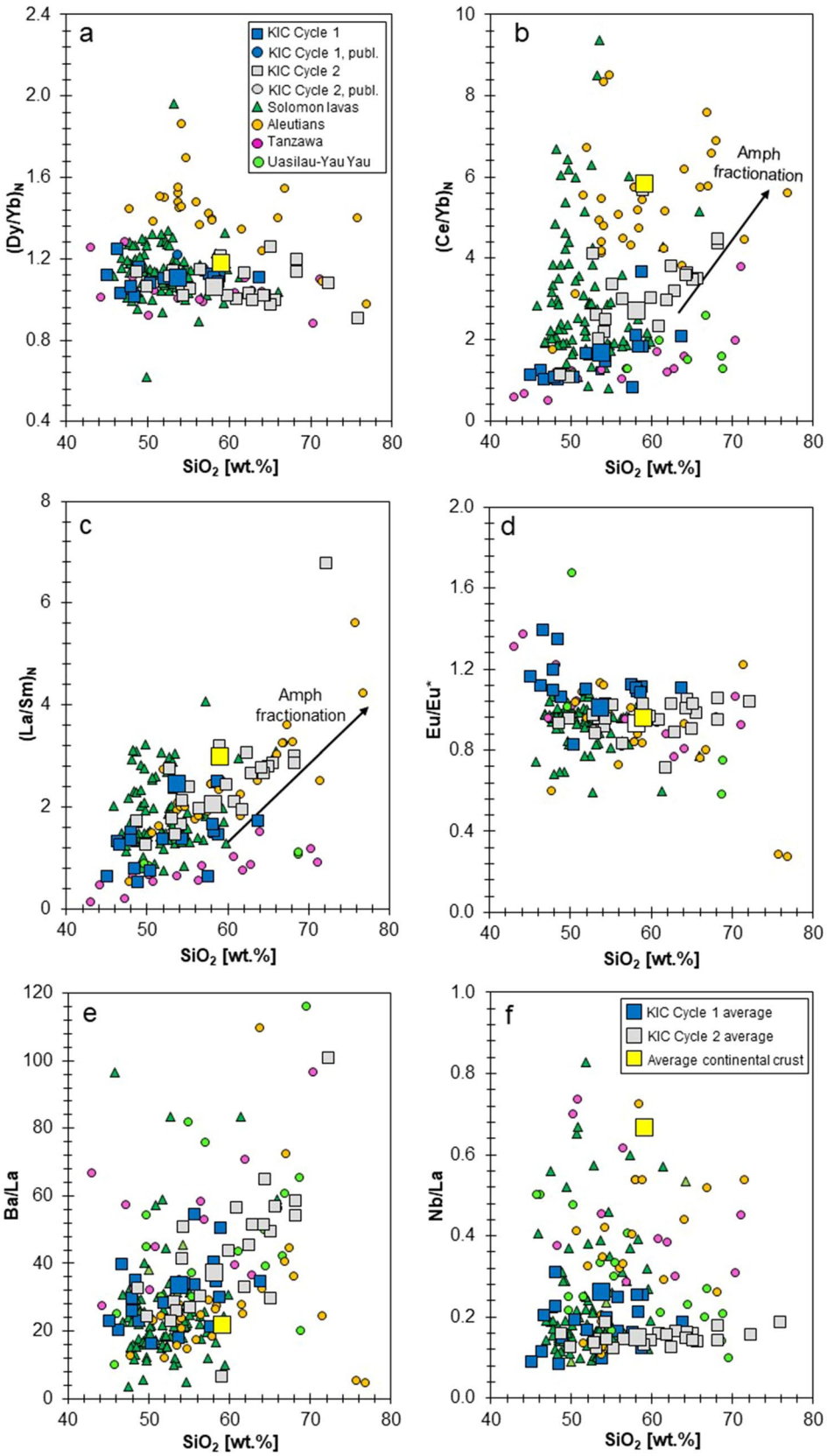

Fig. 6 Trace element variation diagrams for the KIC. **a** $(Dy/Yb)_N$ versus SiO_2 (wt.%). **b** $(Ce/Yb)_N$ versus SiO_2 (wt.%). **c** $(La/Sm)_N$ versus SiO_2 (wt.%). **d** Eu/Eu* versus SiO_2 (wt.%). **e** Ba/La versus SiO_2 (wt.%). **f** Nb/La versus SiO_2 (wt.%). Data sources: Chivas (1977), Chivas et al. (1982), König and Schuth (2011), and Tapster et al. (2016). These diagrams display how the trace element ratio trends of the Cycle 1 and Cycle 2 intrusions compare with one another as well as lavas from the Solomon arc, and plutonic rocks from Cenozoic ultramafic to felsic arc plutons. Data shown for the Solomon arc lavas are from Schuth et al. (2004, 2009), König et al. (2007) and König and Schuth (2011). The Cenozoic arc pluton data sources are the same as those in Fig. 4. The large yellow squares represent the composition of average continental crust from Rudnick (1995). The trace element ratios are normalised to chondrite values from Sun and McDonough (1989)

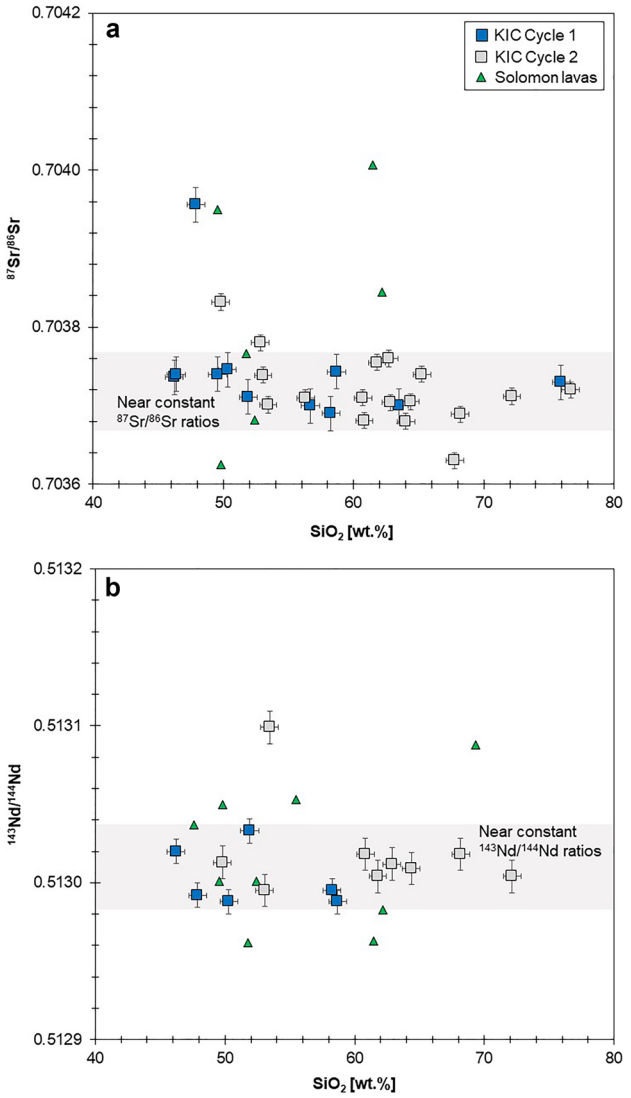

Fig. 7 Radiogenic isotope plots for Cycles 1 and 2 of the KIC, including new data listed in Table S4 and published data in Chivas et al. (1982). **a** $^{87}Sr/^{86}Sr$ versus SiO_2 (wt.%). **b** $^{143}Nd/^{144}Nd$ versus SiO_2 (wt.%). These plots show that the $^{87}Sr/^{86}Sr$ and $^{143}Nd/^{144}Nd$ of the KIC are near constant across a wide compositional range. The radiogenic isotope data in **a** and **b** for the Solomon Island arc lavas are from and König and Schuth (2011). Uncertainty error symbols are shown in this figure

which are not usually regarded as cumulates in the normal sense but liquids. The resultant calculated melt compositions are shown in Fig. 9 and Table S7 and represent the KIC's liquid lines of descent. The calculated fractionation trends closely resemble the KIC major element (MgO, Al_2O_3, CaO and FeO^T vs SiO_2) trends observed in Fig. 4. The calculated fractionation and observed KIC data trends decrease from ~ 8 wt.% MgO at ~ 50 wt.% SiO_2 to ~ 0.5 wt.% MgO at ~ 74 wt.% SiO_2 (Fig. 9). The Al_2O_3 contents of the calculated and observed KIC trends slightly decrease from ~ 18 to 17 wt.% between 49 and 62 wt.% SiO_2 before decreasing more steeply to 13 wt.% at 74 wt.% SiO_2 (Fig. 9). The CaO and FeO^T contents of the calculated and observed KIC trends decrease from ~ 10 wt.% and ~ 12 wt.% at 50 wt.% SiO_2 to 2 wt.% and 1 wt.% at 74 wt.% SiO_2, respectively (Fig. 9). This provides further evidence that the KIC formed by fractional crystallisation of basaltic magmas. The most evolved calculated melt composition (SiO_2 = 74.3 wt.%, Al_2O_3 = 13.0 wt.%, MgO = 0.5 wt.%, CaO = 1.5 wt.%; Na_2O = 3.5 wt.%; Table S7) is very similar to the most evolved felsic lithologies in KIC. The fractionation trend calculated for the KIC and observed in the KIC data is very similar to the low-pressure (0.1 GPa) fractionation trends calculated for the evolution of basaltic arc magmas (Fig. 9) by Loucks (2021). This suggests that KIC magmas fractionated at a shallow depth of ~ 3 km because the KIC data and calculated fractionation trends plot more along the 0.1 GPa trends in Fig. 9 than the high-pressure (1 GPa) trends calculated by Loucks (2021). Experimental and calculated liquid of descent trends determined by Nandedkar et al. (2014) and Bucholz et al. (2014) for basaltic arc magmas fractionating at pressures of 0.7 Ga and 0.2–0.4 GPa do not match the calculated and observed KIC trends to the same extent as the 0.1 GPa fractionation trend of Louck (2021).

Residual sum of squares calculations were conducted using the MINSQ spreadsheet (see S2; Herrmann and Berry, 2002) to establish fractionating mineral proportions for the KIC and further appraise whether this complex formed by fractional crystallisation. This spreadsheet uses whole-rock and mineral compositions to determine the residual sum of squares value between a chosen starting composition and an estimated starting composition and can be applied to various petrological questions. Sample A.498 was chosen as the starting composition because this sample is gabbroic in composition and still represents a melt. Sample A.6 was selected as the evolved sample composition because it has the most evolved composition in Table S3. Representative compositions of plagioclase (An_{60}), olivine (Fo_{78}), amphibole (high Al), clinopyroxene (Mg# = 81), apatite, orthopyroxene (Mg# = 72) and biotite (Mg# = 63) were selected from Table S1 and entered into the spreadsheet. A representative magnetite composition from Chivas (1977) was also incorporated into the spreadsheet. A residual sum of squares value of 1.79 was determined for sample A.498 and the estimated starting composition based on these whole-rock and mineral composition data and the mineral proportions and the remaining melt fraction that were manually entered. This low residual sum of squares value indicates that the geochemical trends observed in the KIC data resulted from fractional crystallisation. The selection of the mineral proportions was based on mineral proportions reported in Kay et al. (2019) for the formation of felsic magmas by fractional crystallisation in the Aleutian arc. Amphibole (41%), plagioclase (31%), clinopyroxene (9%), biotite (3%), magnetite

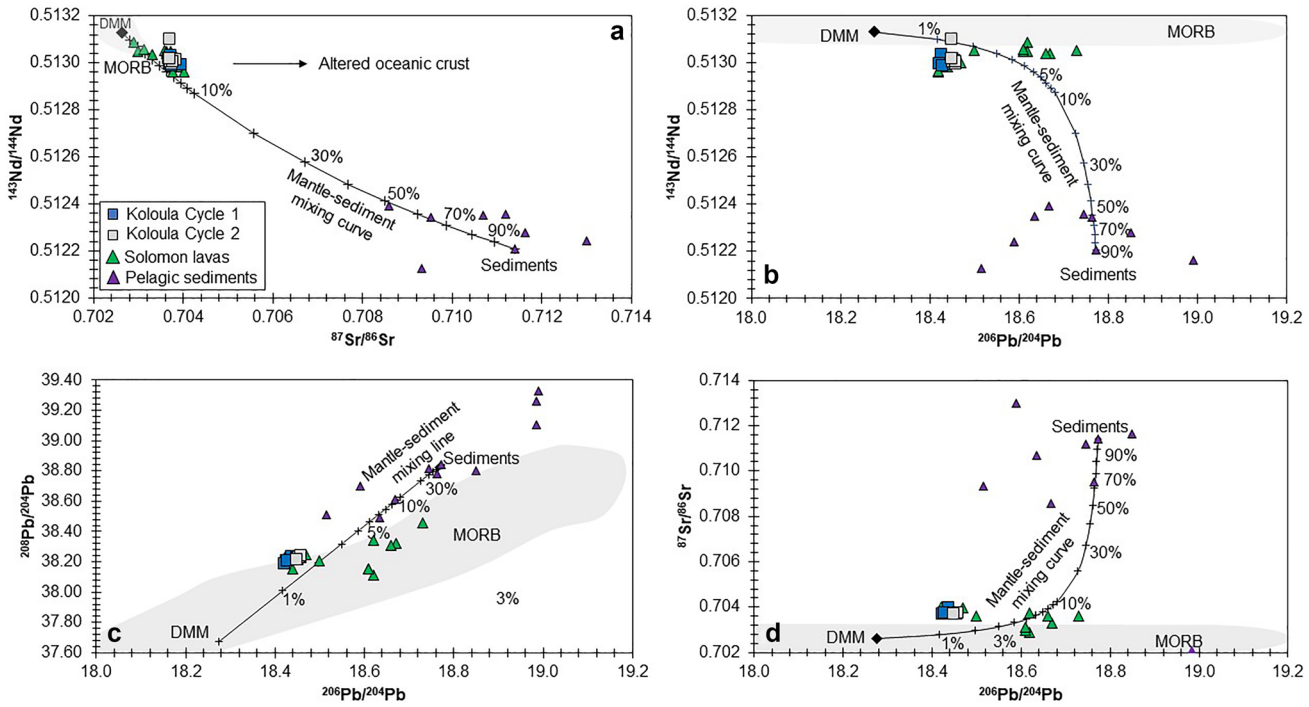

Fig. 8 Mantle–sediment mixing model diagrams for the KIC. **a** $^{143}Nd/^{144}Nd$ versus $^{87}Sr/^{86}Sr$. **b** $^{143}Nd/^{144}Nd$ versus $^{206}Pb/^{204}Pb$. **c** $^{208}Pb/^{204}Pb$ versus $^{206}Pb/^{204}Pb$. **d** $^{87}Sr/^{86}Sr$ versus $^{206}Pb/^{204}Pb$. These diagrams and the MORB fields within them are modified after Kepezhinskas et al. (1997) and Schoenhofen et al. (2020) and show that the radiogenic isotope compositions of the KIC samples can be explained by 1–2% mixing between a depleted MORB mantle (DMM) source and sediment melts. The radiogenic isotope data for the Solomon lavas are shown for comparison and are from König and Schuth (2011). The compositions of the sediment end members are from pelagic sediment data in Ben Othman et al. (1989). The isotopic compositions of DMM are from Workman and Hart (2005). The MORB and sediment fluid compositions used in the generation of the mixing models are from Ayers (1998) and Spandler et al. (2007)

(3%), apatite (2%) and olivine (1%) fractionated from the KIC's parental magma to form the intermediate and felsic lithologies in this complex. These fractionating mineral proportions do not entirely match the modal mineralogy of the mafic to intermediate plutonic rocks in the KIC (e.g. Chivas 1977). However, this is also apparent in the modelling presented by Kay et al. (2019) for the petrogenesis of the Hidden Bay Pluton (Aleutian arc, Alaska) by fractional crystallisation of high-Al basaltic magmas. Kay et al. (2019) found that the basaltic parental magmas to the Hidden Bay Pluton evolved to rhyodacitic and rhyolitic compositions by fractionation of amphibole (44%), plagioclase (35%), clinopyroxene (10%), magnetite (5%), biotite (5%) and apatite (1%). These fractionation mineral proportions are very similar to those found for the KIC.

Evaluation of other differentiation mechanisms proposed for the formation of intermediate to felsic magmas

Tonalitic plutons are commonly found in intra-oceanic island arcs and these felsic magmas are thought to have either formed by shallow fractional crystallisation from mafic melts (e.g. Chivas et al. 1982; Whalen 1985; Haase et al. 2014; Müntener and Ulmer 2018), re-melting of hydrothermally altered mafic crustal rocks and possibly sediments (e.g. Petford and Atherton 1996; Haraguchi et al. 2003; Smith et al. 2003; Saito et al. 2011), lower crustal fractional crystallisation of arc basaltic magmas (Loucks 2021), polybaric fractionation (Almeev et al. 2013; Hamada et al. 2014; Melekhova et al. 2015; Lewis et al. 2021; Marxer et al. 2022), or magma mixing (Eichelberger 1978; Reubi et al. 2003; Reubi and Nicholls 2005; Reubi and Blundy 2009; Ichiyama et al. 2020; Rezeau et al. 2021; Reubi and Müntener 2022).

Tonalites, trondhjemites and granodiorites derived by melting of hydrothermally altered subducting oceanic crust or lower arc crust or by lower crustal fractional crystallisation of hydrous basaltic arc magmas have high Al_2O_3 (≥ 15 wt.%) contents and $(La/Yb)_N$ (≥ 30) and Sr/Y (≥ 30) ratios and low Y (≤ 18 ppm) and Yb (≤ 1.9 ppm) contents reminiscent of adakites (Martin 1986; Drummond and Defant 1990; Petford and Atherton 1996; Hansen et al. 2002; Martin et al. 2005; Loucks 2021). Moreover, the melting of mafic crust near the base of thick (> 40 km) continental arcs has been proposed to account for the high $(La/Yb)_N$ and Sr/Y ratios

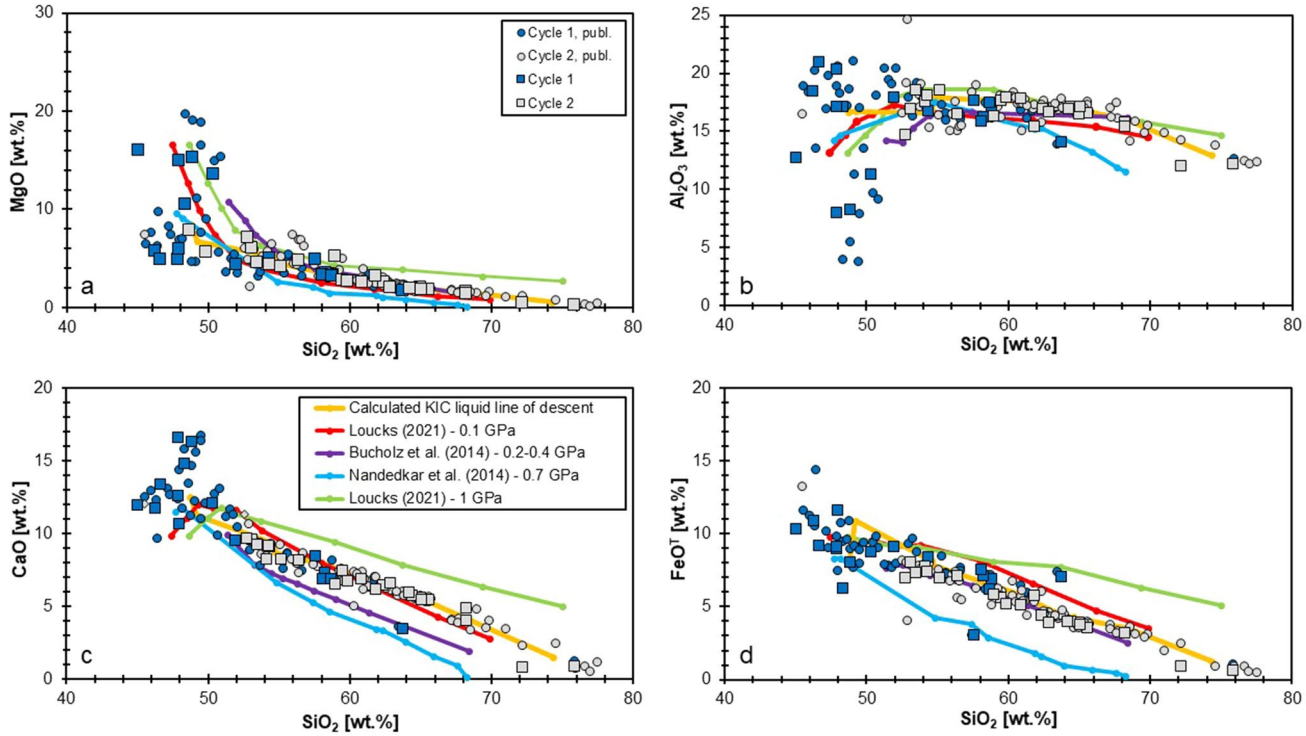

Fig. 9 Calculated liquid line of descent trend diagrams for the KIC. **a** MgO (wt.%), **b** Al_2O_3 (wt.%), **c** CaO (wt.%) and **d** FeO^T (wt.%) versus SiO_2 (wt.%). These calculated liquid line of descent trends were determined using the mass balance equation given in Jagoutz (2010). The modelled high-Al basaltic parental magma to the KIC was used as a starting melting composition. Cumulate compositions were obtained by averaging the compositions of gabbros, quartz diorites, tonalites and aplites from Cycle 2 of the KIC. The calculated fractionation trends plot along the same trends as the KIC samples. Please see the text, Table S2 and Table 7 for more details regarding the mass balance calculations. Liquid lines of descents calculated by Loucks (2021) for basaltic melts crystallising at pressures of 0.1 GPa and 1 GPa are plotted for comparison. The KIC samples plot more along the 0.1 GPa fractionation trend compared to the 1 GPa fractionation trend. Experimental liquid line of descent trends determined by Nandedkar et al. (2014) for primitive, hydrous arc magmas crystallising at 0.7 GPa are also plotted for comparison. Liquid line of descent trends calculated using the mass balance equation in Jagoutz (2010) by Bucholz et al. (2014) for the 0.2–0.4 GPa fractional crystallisation of the Dariv Igneous Complex (Mongolia) are also shown for comparison. The published KIC data are from Table S5 and Table S8

and low Yb and Y concentrations observed in tonalites and granodiorites from continental arc batholiths, such as the Miocene Cordillera Blanca Batholith of Peru (Petford and Atherton 1996). The tonalites from the KIC have $(La/Yb)_N$ ratios of < 10 (2.9–5.8), and most of them have Sr/Y ratios of ≥ 30 (14–64). Moreover, most of the Koloula tonalites have Al_2O_3, Y and Yb contents of ≥ 15 wt.% (15.4–18.2 wt.%), ≤ 18 ppm (7.4–24.9 ppm) and ≤ 2 ppm (0.8–2.6), respectively (Table S3). Moreover, the lack of a correlation between the near-constant $^{143}Nd/^{144}Nd$ isotope ratios (Fig. 7b) and the variable $(La/Sm)_N$ ratios of the KIC indicates that slab-derived sediment melts played a minor role and that the positive correlation between $(La/Sm)_N$ and SiO_2 (Fig. 6c) resulted from amphibole fractionation. The relative thinness (20 km) of the Solomon intra-oceanic island arc crust beneath the KIC indicates that melting of hydrothermally altered subducting oceanic crust or lower arc crust or by lower crustal fractional crystallisation of arc basaltic magmas was unlikely. Furthermore, there is currently no existing field evidence to suggest that the tonalites, trondhjemites and granodiorites of the KIC were derived by in situ melting of mafic arc crust. The low $(La/Yb)_N$ and near-constant $(Dy/Yb)_N$ (~ 1) ratios of the KIC (Fig. 6) indicate that neither garnet nor hornblende was significant residual minerals in its source (e.g. Petford and Atherton 1996; Dessimoz et al. 2012).

Polybaric fractionation has been proposed as a mechanism for the generation of intermediate to felsic magmas in intra-oceanic island arcs and continental arcs (Almeev et al. 2013; Hamada et al. 2014; Melekhova et al. 2015; Lewis et al. 2021; Marxer et al. 2022). Our findings indicate that the lithologies of the KIC formed by fractionation of high-Al basaltic magmas at shallow (0.1 GPa) levels within the Solomon intra-oceanic island arc crust. The similarity of the Sr and Nd isotope ratios of the mafic to felsic rocks of Cycle 1 and Cycle 2 (Fig. 7) suggests that assimilation of sediments or hydrothermally altered crustal material was limited during their magmatic evolution, in agreement with Chivas et al.

(1982). Radiogenic Sr and unradiogenic Nd isotope compositions indicate that there is no old continental material present beneath the KIC, in contrast to the Oligocene Umasani plutonic complex further to the northwest (Fig. 1; Tapster et al. 2014). Moreover, the $\delta^{18}O$ standard mean ocean water (SMOW) isotope values of unaltered whole-rock ultramafic to felsic samples from the KIC range between 5.4 and 7.2‰ (Chivas et al. 1982), indicating that their parental magmas were likely derived from a mantle source and not contaminated by older continental crust (e.g. Valley et al. 1998). The linear trends exhibited by the KIC (Fig. 4) may have resulted from mixing of magmas of different compositions (e.g. Ichiyama et al. 2020; Rezeau et al. 2021); however, the constancy in the $^{143}Nd/^{144}Nd$ and $^{87}Sr/^{86}Sr$ ratios of the KIC ultramafic to felsic lithologies indicates that magma mixing was unlikely (Fig. 7). Additionally, the changing trend from increasing to decreasing P_2O_5 contents with increasing SiO_2 at ca. 56 wt.% SiO_2 (Fig. 4f) indicates that the trends of mafic to felsic magmas cannot reflect binary mixing between these melts.

A new fractional crystallisation model for the KIC

Here, we present a new fractional crystallisation model for the KIC that builds on the findings of Chivas et al. (1982) who proposed that the complex formed by fractional crystallisation. The KIC's primary magmas (11 wt.% MgO) evolved to Al-rich basaltic magmas (6–8 wt.% MgO) through olivine and pyroxene fractionation in the lower crust, most likely at a depth of ~ 20 km at the base of the Solomon intra-oceanic island arc in a manner similar to the model proposed by Kay et al. (2019) for the Hidden Bay and Kagalaska plutons in the Aleutian intra-oceanic island arc. These high-Al basaltic magmas then ascended to the shallow crust to form the KIC. The earliest formed lithology in the KIC constitutes a small proportion of the Cycle 1 intrusions and formed by the crystallisation of olivine and clinopyroxene from the KIC's high-Al basaltic parental magmas. This resulted in the generation of clinopyroxene–olivine cumulates (pyroxenites and olivine pyroxenites) containing 10.6–16.1 wt.% MgO, representing the earliest formed lithologies in the KIC and the crystallisation of pyroxenites in the shallow crust (Chivas and McDougall 1978; Chivas et al. 1982). The more primitive nature of the high-Al basaltic magmas intruding the shallow crust during Cycle 1 compared to Cycle 2 is supported by the An-rich composition ($> An_{90}$) of plagioclase in the Cycle 1 pyroxenites (Fig. 3). The decreasing An contents in each cycle likely reflect increasing magma evolution beginning with the most mafic composition. Lavas from Savo contain abundant xenoliths of clinopyroxenites (Smith 2014) that likely represent cumulates from shallow magma chambers comparable to that of the KIC. Moreover, amphibole in amphibole cumulates beneath arc volcanoes on Savo probably formed by reaction replacement of earlier formed clinopyroxene, orthopyroxene, olivine, plagioclase, and Fe–Ti oxides (Smith 2014). The olivine compositions of the Koloula pyroxenites (Fo_{75-82}) indicate that their parental magmas (Mg# = 50–60) were ~ 23–50% more evolved than primary magmas (Mg# = 74) with more primitive olivine (Fo_{90}) compositions (Table S1; e.g. Almeev et al. 2007). On the other hand, the olivine compositions of the Koloula pyroxenites suggest that melts with Mg# of 50–60 ascended into the upper crust of the Solomon island arc. Following the crystallisation of the KIC pyroxenites, plagioclase, pyroxene and, to a lesser extent, olivine fractionated from the KIC's high-Al basaltic magmas to form the anorthositic segregations, leucogabbros, gabbros and pyroxenites in the Chakachaka Gabbro.

Shallow (0.1 GPa) fractionation of olivine, clinopyroxene, plagioclase, amphibole, biotite, apatite and Fe–Ti oxides from the KIC high-Al basaltic magmas resulted in the generation of calc-alkaline magmas in the Solomon intra-oceanic island arc beneath Guadalcanal and the formation of the intermediate-felsic plutonic rocks of the KIC (Figs. 4, 6 and 9; Table S7). The crystallisation of olivine, clinopyroxene, plagioclase and Fe-Ti oxides led to a significant decrease in MgO, CaO and FeO^T contents with increasing SiO_2 (Fig. 4). Similar trends are observed in rocks from other Cenozoic ultramafic to felsic arc plutons, such as the Tanzawa Plutonic Complex and Uasilau-Yau Yau Intrusive Complex, which formed in the comparable settings of the Izu–Bonin–Mariana and Bismarck island arcs, respectively (Fig. 4; Whalen 1985; Kawate and Arima 1998; Suzuki et al. 2015). The Al_2O_3 contents of the KIC samples started to gently decrease at ~ 49 wt.% SiO_2, marking the onset of plagioclase crystallisation. The crystallisation of plagioclase is reflected by the positive Eu/Eu* anomaly ratios exhibited by some Cycle 1 samples, which represent plagioclase-rich cumulates (Fig. 6). The Na_2O contents of the KIC decreased with increasing SiO_2 due to the crystallisation of An-rich plagioclase and amphibole.

Hornblende fractionation is known to be important for the formation of calc-alkaline magmas (Sisson and Grove 1993a, b; Davidson et al. 2007) and has been shown to occur in the deep roots of thick (> 40 km) continental arcs, as observed in the Cretaceous (120–100 Ma) Chelan Complex of the Cascades arc in Washington, USA (Dessimoz et al. 2012). The increasing $(La/Sm)_N$ and $(Ce/Yb)_N$ ratios of the KIC with increasing SiO_2 (Fig. 6), and the occurrence of abundant amphibole (10–30%) in the mafic and intermediate lithologies of the KIC suggest that hornblende fractionation played a significant role in the formation of the complex's calc-alkaline intermediate to felsic plutonic rocks (Chivas 1977; Davidson et al. 2007; Smith 2014). This indicates that significant amphibole fractionation can occur in thin, ca. 20 km-thick intra-oceanic island arcs, such as the Solomon

arc. The crystallisation of amphibole after the KIC magmas had attained SiO_2 contents of > 60 wt.% led to a decrease in MgO, Al_2O_3, CaO and FeO^T contents with increasing SiO_2. This amphibole fractionation likely occurred after olivine (MgO) and plagioclase (Al_2O_3) fractionation yet overlapped with clinopyroxene and plagioclase (CaO), and biotite and Fe–Ti oxide (FeO^T) fractionation (e.g. Loucks, 2021). The occurrence of abundant biotite (4–16%) in the mafic to intermediate plutonic rocks of the KIC (Chivas 1977) imply that biotite fractionation played a role in the formation of this complex. Biotite fractionation led to a decrease in the Al_2O_3, FeO^T and MgO contents of the KIC with increasing SiO_2 (Fig. 4). Apatite fractionation commenced at ~ 60 wt.% SiO_2, leading to a decrease in the P_2O_5 contents of the KIC magmas and an upside-down V-shaped trend in the KIC data (Fig. 4).

The basaltic composition of the parental magmas of the KIC evolved to andesitic, dacitic and rhyolitic compositions by fractional crystallisation (Figs. 4 and 6). The crystallisation of successively more evolved lithologies (gabbro, diorite, quartz diorite, tonalite, granodiorite and aplite) drove the evolution of the KIC magmas to increasingly more evolved compositions. This was manifested by the successive crystallisation of the Kolochoro Quartz Diorite, Kolokemau Tonalite, Vurakara Quartz Diorite, Charilava Quartz Diorite, melanocratic tonalite, tonalite 1, tonalite 2, porphyritic tonalite, tonalite 3, Chikora Tonalite Porphyry and aplite dykes. The bulk basaltic and andesitic compositions of Cycle 1 and Cycle 2 (Figs. 4 and 6), respectively, were calculated by averaging the respective compositions of the Cycle 1 and Cycle 2 samples, the latter being similar to that of the andesitic composition of the average continental crust (Rudnick 1995; Hawkesworth et al. 2010). Moreover, the bulk andesitic composition of Cycle 2 is very similar to the compositions of the andesite dykes that are exposed in the KIC and were mostly emplaced after the crystallisation of the Inamumu Zoned Pluton (Table S3 and Table S5). These dykes provide further evidence for the evolution of the KIC magmas from basaltic to more evolved compositions.

Variation of slab input into the primary magmas of the KIC

The distinctive Nd, Pb and Sr isotope ratios of the Cycle 1 and 2 intrusions indicate that they may have formed by partial melting of a sub-arc mantle source (Chivas et al. 1982) that was variably enriched by slab-derived melts and/or fluids. The more radiogenic Pb isotope compositions and higher Ba/La and $(Ce/Yb)_N$ and lower Nb/La ratios of the Cycle 2 intrusions compared to the Cycle 1 intrusions suggest that the former was derived by partial melting of a similar sub-arc mantle source that was more re-enriched by LILE and LREE-rich slab-derived melts and/or fluids (Hawkesworth et al. 1991; Kent and Elliott 2002).

The slab-derived melts may have been generated as a consequence of the partial melting of subducting basaltic oceanic crust and/or sediments. Mantle-sediment mixing modelling based on the Nd, Pb and Sr isotopic compositions of the KIC, pelagic marine sediments and depleted MORB mantle (DMM) indicates that the KIC's primary magmas were derived from a DMM-like mantle source with a minor (1–2%) contribution of slab-derived sediment melts to the sub-arc mantle source(s) of the KIC (Fig. 8; Kepezhinskas et al. 1997; Schoenhofen et al. 2020). There is no evidence for melting of subducting altered oceanic crust because the $(Dy/Yb)_N$ ratios are low and do not show input of melts from a source with residual garnet, e.g. from eclogite (Figs. 6 and 8). Based on their $^{206}Pb/^{204}Pb$ ratios, the Cycle 2 intrusions had a slightly greater contribution of slab-derived Pb via melts or fluids in their sub-arc mantle source than the Cycle 1 intrusions (Fig. 8). However, the overlapping $^{87}Sr/^{86}Sr$ and $^{143}Nd/^{144}Nd$ ratios of Cycles 1 and 2 suggest that the amount of sediment melt input did not change significantly between these cycles (Fig. 7). The Cycle 2 intrusions were more influenced by slab-derived sediment melts than the Cycle 1 intrusions (Fig. 8). The sub-arc mantle source of the Cycle 2 intrusions was more enriched in LILE and HFSE and had higher LREE contents, and $^{206}Pb/^{204}Pb$ and $^{208}Pb/^{204}Pb$ isotopic ratios compared to the sub-arc mantle source of the Cycle 1 intrusions (Figs. 5, 6, 7 and 8). This suggests that the parental magmas to the KIC were derived by partial melting of a heterogeneous depleted mantle source that may have been re-enriched with distinct slab-derived sediment melts to various extents. Slab-derived sediment melts also played a minor role (1–3%) in the genesis of lavas from the Solomon arc (Fig. 8; e.g. Kepezhinskas et al. 1997; König et al. 2007). There are some minor differences between the N-MORB-normalised trace element patterns of the KIC and the lavas from the Solomon arc (Fig. 5). These differences may be due to the respective locations of the other Solomon Islands between the inactive Vitiaz and active San Cristobal trenches and the consequent varying interactions between both subduction zones beneath these islands (e.g. Smith et al. 2009).

Comparison of the KIC with ultramafic to felsic plutons in Cenozoic intra-oceanic island arcs

Ultramafic to felsic plutons similar to the KIC occur in other Cenozoic intra-oceanic island arcs in the Pacific Ocean, such as the Izu–Bonin–Mariana, Aleutian, Vitiaz and Bismarck island arcs (Whalen 1985; Kawate and Arima 1998; Suzuki et al. 2015; Kay et al. 2019; Marien et al. 2022). These plutons show similar whole-rock compositional ranges from pyroxenites and gabbros to diorites, tonalites, and granodiorites. They also show similar major and incompatible element

variations with SiO_2 contents to the KIC and comparable N-MORB-normalised trace element ratios (Figs. 4, 5 and 6; Table S8). Thus, we suggest that very similar processes dominated by fractional crystallisation formed intermediate and felsic magmas from mafic melts, which is in agreement with the majority of studies on these plutons (Whalen 1985; Kay et al. 2019; Marien et al. 2022). The oldest rocks in the KIC and Uasilau-Yau Yau Intrusive Complex on the island of New Britain in the Bismarck island arc are gabbros (Fig. 4) and it appears that the more evolved rocks in Cenozoic ultramafic to mafic plutons represent magmas that formed from these initial mafic melts. Thus, the evolved compositions are generally less abundant than the gabbros. Amphibole fractionation causes an increase in $(La/Sm)_N$ and decrease in $(Dy/Yb)_N$ with increasing SiO_2 contents (Davidson et al. 2007; Smith 2014), which is observed to a variable extent in all of the aforementioned Cenozoic ultramafic to felsic arc plutons (Fig. 6; e.g. Whalen 1985; Kawate and Arima 1998; Suzuki et al. 2014, 2015; Kay et al. 2019; Marien et al. 2022).

The Miocene–Pliocene (8.9–4.0 ± 0.2 Ma) Tanzawa Plutonic Complex in the active Izu–Bonin–Mariana intra-oceanic arc of Japan has been proposed to have formed by partial melting of mafic lower arc crust (Kawate and Arima 1998; Suzuki et al. 2014, 2015). However, the mostly linear trends exhibited by the Tanzawa Plutonic Complex are very similar to those displayed by the KIC (Fig. 4) and are most easily explained by fractional crystallisation processes given that we have ruled out other processes for the latter. The great similarity in the petrology and major and trace element geochemistry of the Tanzawa Plutonic Complex and KIC indicates that these young intra-oceanic island arc-derived plutonic complexes most likely formed by the same process. Additionally, Suzuki et al. (2015) found that most $\delta^{18}O$ zircon isotope values of the Tanzawa tonalites were in the range of 5.3 ± 0.3‰, indicating equilibrium with the mantle (Valley et al. 1998), which are similar to the mantle-like whole-rock $\delta^{18}O$ compositions (5.4 to 7.2‰) of the KIC (Chivas et al. 1982). The highest $\delta^{18}O$ compositions (> 6.0‰) from the KIC can be attributed to temperature-dependent fractionation of oxygen isotopes (Chivas et al. 1982). Only a few Tanzawa samples have low $\delta^{18}O$ zircon isotope values that could be due to melting of hydrothermally altered oceanic arc crust (Suzuki et al. 2015).

The Late Oligocene–Early Miocene (34.6–30.9 ± 0.4 Ma) Hidden Bay and Middle Miocene (14.7–13.9 ± 0.3 Ma) Kagalaska plutons are located in the active central Aleutian intra-oceanic island arc in Alaska, USA, and had initially basaltic melts, containing ~ 7.6 wt.% MgO, that fractionated olivine, clinopyroxene and pargasitic amphibole at ~ 12 km depth leading to the emplacement of predominantly granodioritic magma(s) into the shallow crust at depths of 2–4 km (Kay et al. 2019). The initial basaltic magma of Cycle 1 intruded the shallow crust at the KIC had > 5 wt.% MgO, thus resembling the processes observed in the Aleutian island arc. As is the case with the KIC, the MgO, CaO and FeO^T contents of the Aleutian plutons decrease with increasing SiO_2, signifying olivine, clinopyroxene, amphibole, plagioclase, biotite, and Fe–Ti oxide fractionation (Fig. 4; Kay et al. 2019). The Al_2O_3 contents of the Aleutian plutons also gently decrease from ~ 18 to ~ 17 wt.% between ~ 49 and ~ 62 wt.% SiO_2 (plagioclase fractionation) before decreasing more steeply (amphibole and biotite fractionation). Moreover, the Na_2O contents of the Aleutian plutons increase with increasing SiO_2, indicating plagioclase and amphibole fractionation. The P_2O_5 contents of the KIC and Aleutian plutons increase between ~ 49 and ~ 56 wt.% SiO_2 before decreasing due to the onset of apatite fractionation (Fig. 4).

The $(La/Sm)_N$ and $(Ce/Yb)_N$ ratios of the KIC and Aleutian plutons increase with increasing SiO_2, pointing to amphibole fractionation (Fig. 6). The Aleutian arc is approximately 37 km-thick beneath the Hidden Bay and Kagalaska plutons (Kay et al. 2019), almost twice the thickness of the 20 km-thick Solomon intra-oceanic island arc crust beneath the KIC; therefore, hornblende fractionation would have been more likely in the thicker arc crust of the former (Petford and Atherton 1996; Dessimoz et al. 2012). This is borne out by the more distinctive decrease in the $(Dy/Yb)_N$ ratios with increasing SiO_2 in the Aleutian plutons compared to the KIC (Fig. 6). Moreover, the Aleutian plutons have higher $(Dy/Yb)_N$ and $(Ce/Yb)_N$ ratios at a given SiO_2 content than the KIC (Fig. 6).

It has been proposed that island arcs exhibit chemical stratification; however, this has only been shown for arc crust thicker than ~ 35–40 km, such as the Triassic–Jurassic Talkeetna arc, Alaska, and the Cretaceous-Eocene Kohistan arc in Pakistan (Greene et al. 2006; Jagoutz 2014). Chemical stratification models suggest that mafic lower crust and felsic upper crust formed early in the magmatic evolution of island arcs through the fractionation of ferromagnesian minerals from mafic magmas in the deep crust followed by the ascent of intermediate to felsic melts to the middle to upper crust (Annen et al. 2006; Greene et al. 2006; Jagoutz 2014). The Talkeetna and Kohistan arcs display this chemical stratification, with SiO_2, K_2O and Th/La decreasing with depth and CaO and MgO increasing with increasing depth (Table S8; Rioux 2006; Greene et al. 2006; Rioux et al. 2010; Jagoutz 2014).

The aforementioned Cenozoic ultramafic-felsic arc plutons have similar mineral assemblages, mineral (Mg-rich olivine, pyroxene and calcic plagioclase) and whole-rock compositions and emplacement depths, and all intruded into shallow (< 10 km) mafic island arc crust (Figs. 4, 5 and 6; see Chivas et al. 1982; Whalen 1985; Kawate and Arima 1998; Suzuki et al. 2015; Tapster et al. 2016; Kay et al. 2019; Marien et al. 2022). The Fo contents and Mg#

numbers of olivine and clinopyroxene from the KIC and other Cenozoic arc plutons indicate that Mg-rich basaltic magmas with Mg# > 50–60 were emplaced into shallow island arc crust. The decreased density of high-Al basaltic magmas resulting from prior olivine and clinopyroxene fractionation and the similar density of the mafic island arc crust into which the ultramafic-felsic plutons intruded would have made their emplacement at shallow depths (< 10 km) more likely (e.g. Herzberg et al. 1983). This implies that the thickness, composition and age of arc crust govern whether ultramafic-felsic magmas can ascend to the shallow island arc crust. This may explain why the ultramafic to felsic KIC, Tanzawa Plutonic Complex and Uasilau-Yau Yau Intrusive Complex and Hidden Bay, Kagalaska, Colo, Yavuna and Momi plutons, are found in shallow island arc crust (< 10 km), whereas the Kohistan and Talkeetna arcs are chemically stratified (e.g. Rasmussen et al. 2022). This also shows that shallow fractional crystallisation of mantle-derived basaltic magmas is an important crustal growth process in intra-oceanic arcs.

The magma reservoirs beneath active island arc volcanoes have been seismically detected at depths of 3–11 km (Tsuruga et al. 2006; Allard et al. 2016; Paulatto et al. 2019; Janiszewski et al. 2020; Yukutake et al. 2021), i.e. comparable to the intrusion depths of the aforementioned plutons. We suggest that the plutons studied here represent the fossil magma systems of arc volcanoes, which is supported by the fact that the Solomon arc lavas closely resemble the KIC plutonic rocks (Figs. 4, 5 and 6), indicating a close relationship between volcanic and plutonic rocks in the Solomon island arc. Therefore, the shallow island arc crust grows by multiple magma intrusion cycles beneath volcanoes and by the migration of magmatism with time.

Conclusions

(1) The Koloula Igneous Complex is divided into Cycle 1 and 2 intrusions, each representing a calc-alkaline liquid line of descent caused by the fractionation of olivine, clinopyroxene, plagioclase, amphibole, biotite, apatite, and Fe–Ti oxides. The continuous fractionation towards more evolved compositions within each cycle is recorded by the bulk rock compositional data and is also supported by decreasing An contents in plagioclase. Shallow Cenozoic plutons in other young Pacific islands arcs also show evidence for fractional crystallisation as the main process of magma evolution, implying that this process dominates crustal growth in intra-oceanic island arcs.

(2) Abundant hornblende and increasing $(La/Sm)_N$ and $(Ce/Yb)_N$ ratios with increasing SiO_2 in the KIC and other Cenozoic arc plutons demonstrate that hornblende fractionation played a variably significant role in the genesis of their calc-alkaline felsic plutonic rocks, generating felsic magmas with an enrichment of light REE.

(3) The KIC formed by fractional crystallisation of basaltic parental magmas with 6–8 wt.% MgO that intruded at a depth of ~ 2.0–3.0 km (~ 0.1 GPa), i.e. similar to the depths determined for other intrusions in young Pacific island arcs.

(4) Magmas of the Koloula Igneous Complex neither show evidence for crustal assimilation during fractional crystallisation nor is there evidence for the formation of the magmas by partial melting of mafic lower arc crust.

(5) The parental magmas of the Koloula Igneous Complex were derived through hydrous melting of depleted MORB mantle sources that was enriched by slab-derived sediment melts (~ 1-2%) and fluids. The mantle source of the Cycle 2 magmas was slightly more affected by slab-derived sediment melts and fluids with a distinct Pb isotope signature compared to the Cycle 1 intrusions.

(6) Ultramafic to felsic plutons in Cenozoic intra-oceanic island arcs in the Pacific resemble the composition of arc lavas and are thus the fossil roots of arc volcanic systems. The formation and emplacement of ultramafic to mafic plutonic rocks at shallow depths (< 5 km) imply a relatively mafic upper island arc crust in contrast to the chemical stratification of thicker arcs. This also permitted the ascent of basaltic magmas to shallow depths.

Supplementary Information The online version contains supplementary material available at https://doi.org/10.1007/s00410-022-01972-z.

Acknowledgements We thank Melanie Hertel and Marcel Regelous for help with the analytical work. This research is supported by an Alexander von Humboldt Foundation Postdoctoral Research Fellowship awarded to Paul Sotiriou. We would like to thank Othmar Müntener for his professional editorial handling of our manuscript. We are also grateful to Felix Marxer and Madeline Lewis for their insightful and constructive reviews.

Funding Open Access funding enabled and organized by Projekt DEAL.

Data availability statement All data generated or analysed during this study are included in this published article (and its supplementaryinformation files).

Declarations

Conflict of interest The authors declare that they have no known competing financial interests or personal relationships that could have appeared to influence the work reported in this paper.

References

Allard P, Aiuppa A, Bani P, Métrich N, Bertagnini A, Gauthier P-J, Shinohara H, Sawyer G, Parello F, Bagnato E, Pelletier B, Garaebiti E (2016) Prodigious emission rates and magma degassing budget of major, trace and radioactive volatile species from Ambrym basaltic volcano, Vanuatu island arc. J Volcanol Geoth Res 322:119–143

Almeev RR, Holtz F, Koepke J, Parat F, Botcharnikov RE (2007) The effect of H_2O on olivine crystallization in MORB: experimental calibration at 200 MPa. Am Mineral 92:670–674

Almeev RR, Ariskin AA, Kimura JI, Barmina GS (2013) The role of polybaric crystallization in genesis of andesitic magmas: phase equilibria simulations of the Bezymianny volcanic subseries. J Volcanol Geoth Res 263:182–192

Annen C, Blundy JD, Sparks RSJ (2006) The genesis of intermediate and silicic magmas in deep crustal hot zones. J Petrol 47:505–539

Ariskin AA, Barmina GS, Frenkel MY (1987) Computer simulation of basalt magma crystallization at a fixed oxygen fugacity. Geochem Int 24:85–98

Ayers J (1998) Trace element modeling of aqueous fluid – peridotite interaction in the mantle wedge of subduction zones. Contrib Mineral Petrol 132:390–404

Ben Othman D, White MW, Patchett J (1989) The geochemistry of marine sediments, island arc magma genesis, and crust-mantle recycling. Earth Planet Sci Lett 94:1–21

Bodnar RJ, Burnham CW, Sterner SM (1985) Synthetic fluid inclusions in natural quartz. III. Determination of phase equilibrium properties in the system H_2O-NaCl to 1000 °C and 1500 bars. Geochim Cosmochim Acta 49:1861–1873

Bucholz CE, Jagoutz O, Schmidt MW, Sambuu O (2014) Fractional crystallization of high-K arc magmas: biotite-versus amphibole-dominated fractionation series in the Dariv Igneous Complex, Western Mongolia. Contrib Mineral Petrol 168(5):1–28

Chivas AR (1977) Geochemistry, geochronology and fluid inclusion studies of porphyry copper mineralization at the Koloula Igneous Complex, Guadalcanal, Solomon Islands. PhD dissertation, University of Sydney. https://ses.library.usyd.edu.au/handle/2123/5012.

Chivas AR (1978) Porphyry copper mineralization at the Koloula Igneous Complex, Guadalcanal, Solomon Islands. Econ Geol 73:645–677

Chivas AR (1981) Geochemical evidence for magmatic fluids in porphyry copper mineralization. Part I. Mafic silicates from the Koloula Igneous Complex. Contrib Mineral Petrol 78:389–403

Chivas AR, McDougall I (1978) Geochronology of the Koloula porphyry copper prospect, Guadalcanal, Solomon Islands. Econ Geol 73:678–689

Chivas AR, Wilkins RWT (1977) Fluid inclusion studies in relation to hydrothermal alteration and mineralization at the Koloula porphyry copper prospect, Guadalcanal. Econ Geol 72:153–169

Chivas AR, Andrew AS, Sinha AK, O'Neil JR (1982) Geochemistry of a Pliocene-Pleistocene oceanic-arc plutonic complex, Guadalcanal. Nature 300:139–143. https://doi.org/10.1038/300139a0

Compston W, Oversby VM (1969) Lead isotopic analysis using a double spike. J Geophys Res 74:4338–4348

Danyushevsky LV, Plechov P (2011) Petrolog 3: integrated software for modelling crystallization processes. Geochem Geophys Geosystem. https://doi.org/10.1029/2011gc003516

Davidson J, Turner S, Handley H, Macpherson C, Dosseto A (2007) Amphibole "sponge" in arc crust? Geology 35:787–790

DeBari SM (1997) Evolution of magmas in continental and oceanic arcs: the role of the lower crust. Can Mineral 35:501–520

Dessimoz M, Müntener O, Ulmer P (2012) A case for hornblende dominated fractionation of arc magmas: the Chelan Complex (Washington Cascades). Contrib Mineral Petrol 163:567–589

Drummond MS, Defant MJ (1990) A model for trondhjemite-tonalite-dacite genesis and crustal growth via slab melting: Archean to modern comparisons. J Geophys Res 95:21503–21521

Eichelberg JC (1978) Andesitic volcanism and crustal evolution. Nature 275:21–27

Freund S, Beier C, Krumm S, Haase KM (2013) Oxygen isotope evidence for the formation of andesitic-dacitic magmas from the fast-spreading Pacific-Antarctic Rise by assimilation-fractional crystallization. Chem Geol 347:271–283. https://doi.org/10.1016/j.chemgeo.2013.04.013

Furumoto AS, Hussong DM, Campbell JF, Sutton GH, Malahoff A, Rose JC, Woollard GP (1970) Crustal and upper mantle structure of the Solomon Islands as revealed by seismic refraction survey of November-December 1966. Pac Sci 24:315–332

Greene AR, DeBari SM, Kelemen PB, Blusztajn J, Clift PD (2006) A detailed geochemical study of island arc crust: the Talkeetna Arc section, south-central Alaska. J Petrol 47:1051–1093

Haase KM, Lima S, Krumm S, Garbe-Schönberg D (2014) The magmatic evolution of young island arc crust observed in gabbroic to tonalitic xenoliths from Raoul Island, Kermadec Island Arc. Lithos 210–211:199–208. https://doi.org/10.1016/j.lithos.2014.10.005

Haase KM, Beier C, Regelous M, Rapprich V, Renno A (2017) Spatial variability of source composition and petrogenesis in rift and rift flank alkaline lavas from the Eger Rift, Central Europe. Chem Geol 455:304–314. https://doi.org/10.1016/j.chegeo.2016.11.003

Hackman BD (1978) Geological map of Guadalcanal Solomon Islands. Institute of Geological Sciences, London, UK (**scale 1:150,000**)

Hamada M, Okayama Y, Kaneko T, Yasuda A, Fujii T (2014) Polybaric crystallization differentiation of H_2O-saturated island arc low-K tholeiite magmas: a case study of the Izu-Oshima volcano in the Izu arc. Earth Planets Space 66:1–10

Hansen J, Skjerlie KP, Pederson RB, De La Rosa J (2002) Crustal melting in the lower parts of island arcs: an example from the Bremanger Granitoid Complex, west Norwegian Caledonides. Contrib Mineral Petrol 143:316–335

Haraguchi S, Ishii T, Kimura J-I, Ohara Y (2003) Formation of tonalite from basaltic magma at the Komahashi-Daini Seamount, northern Kyushu-Palau Ridge in the Philippine Sea, and growth of Izu-Ogasawara (Bonin)-Mariana arc crust. Contrib Mineral Petrol 145:151–168

Hawkesworth CJ, Hergt JM, Ellam RM, McDermott F (1991) Element fluxes associated with subduction related magmatism. Philos T Roy Soc A 335:393–405

Hawkesworth CJ, Dhuime B, Pietranik AB, Cawood PA, Kemp AIS, Storey CD (2010) The generation and evolution of the continental

crust. J Geol Soc, London 167:229–248. https://doi.org/10.1144/0016-76492009-072
Herrmann W, Berry RF (2002) MINSQ – a least squares spreadsheet method for calculating mineral proportions from whole rock major element analyses. Geochem Explor Environ Anal 2:361–368
Herzberg CT, Fyfe WS, Carr MJ (1983) Density constraints on the formation of the continental Moho and crust. Contrib Mineral Petrol 84:1–5
Holbrook WS, Lizzaralde D, McGeary S, Bangs N, Diebold JB (1999) Structure and composition of the Aleutian island arc and implications for continental crustal growth. Geology 27:31–34. https://doi.org/10.1130/0091-7613(1999)027%3c0031:SACOTA%3e2.3.CO;2
Holm RJ, Tapster S, Jelsma HA, Rosenbaum G, Mark DF (2019) Tectonic evolution and copper-gold metallogenesis of the Papua New Guinea and Solomon Islands region. Ore Geol Rev 104:208–226. https://doi.org/10.1016/j.oregeorev.2018.11.007
Ichiyama Y, Ito H, Tamura A, Arai S (2020) Magma mixing model for the genesis of middle crust in the Izu-Bonin-Mariana arc: evidence from plutonic rocks in the Mineoka-Setogawa ophiolitic mélange, central Japan. Int Geol Rev 62:503–521
Jagoutz OE (2010) Construction of the granitoid crust of an island arc. Part II: a quantitative petrogenetic model. Contrib Mineral Petrol 160:359–381.
Jagoutz O (2014) Arc crustal differentiation mechanisms. Earth Planet Sci Lett 396:267–277
Janiszewski HA, Wagner LS, Roman DC (2020) Aseismic mid-crustal magma reservoir at Cleveland Volcano imaged through novel receiver function analyses. Sci Rep 10:780. https://doi.org/10.1038/s41598-020-58589-0
Kawate S, Arima M (1998) Petrogenesis of the Tanzawa plutonic complex, central Japan: exposed felsic middle crust of the Izu-Bonin-Mariana arc. Isl Arc 7:342–358
Kay SM, Jicha BR, Citron GL, Kay RW, Tibbetts AK, Rivera TA (2019) The calc-alkaline Hidden Bay and Kagalaska plutons and the construction of the Central Aleutian oceanic arc crust. J Petrol 80:393–439
Keith M, Haase KM, Chivas AR, Klemd R (2022) Phase separation and fluid mixing revealed by trace element signatures in pyrite from porphyry systems. Geochim Cosmochim Acta 329:185–205
Kent AJ, Elliott TR (2002) Melt inclusions from Marianas arc lavas: implications for the composition and formation of island arc magmas. Chem Geol 183:263–286
Kepezhinskas P, McDermott F, Defant MJ, Hochstaedter A, Drummond MS, Hawkesworth CJ, Koloskov A, Maury RC, Bellon H (1997) Trace element and Sr-Nd-Pb isotopic constrains on a three-component model of Kamchatka arc petrogenesis. Geochim Cosmochim Acta 61:577–600
König S, Schuth S (2011) Deep melting of old subducted oceanic crust recorded by superchondritic Nb/Ta in modern island arc lavas. Earth Planet Sci Lett 301:265–274
König S, Schuth S, Münker C, Qopoto C (2007) The role of slab melting in the petrogenesis of high-Mg andesites: evidence from Simbo Volcano, Solomon Islands. Contrib Mineral Petrol 153:85–103
Lee CTA, Tang M (2020) How to make porphyry copper deposits. Earth Planet Sci Lett 529:115868. https://doi.org/10.1016/j.epsl.2019.115868
Lewis MJ, Bucholz CE, Jagoutz OE (2021) Evidence for polybaric fractional crystallization in a continental arc: Hidden Lakes mafic complex, Sierra Nevada batholith, California. Contrib Mineral Petrol 176:1–27
Loucks RR (2021) Deep entrapment of buoyant magmas by orogenic tectonic stress: Its role in producing continental crust, adakites, and porphyry copper deposits. Earth-Sci Rev 220:103744. https://doi.org/10.1016/j.earscirev.2021.103744
Marien CS, Drewes-Todd EK, Stork A, Todd E, Gill JB, Hoffmann JE, Tani K, Allen CM, Münker C (2022) Juvenile continental crust evolution in a modern oceanic arc setting: petrogenesis of Cenozoic felsic plutons in Fiji, SW Pacific. Geochim Cosmochim Acta 320:339–365. https://doi.org/10.1016/j.gca.2021.11.033
Martin H (1986) Effect of steeper Archean geothermal gradient on geochemistry of subduction zone magmas. Geology 14:753–756
Martin H, Smithies RH, Rapp R, Moyen J-F, Champion D (2005) An overview of adakite, tonalite-trondhjemite-granodiorite (TTG), and sanukitoid: relationships and some implications for crustal evolution. Lithos 79:1–24
Marxer F, Ulmer P, Müntener O (2022) Polybaric fractional crystallisation of arc magmas: an experimental study simulating transcrustal magmatic systems. Contrib Mineral Petrol 177:1–36
Melekhova E, Blundy J, Robertson R, Humphreys MC (2015) Experimental evidence for polybaric differentiation of primitive arc basalt beneath St. Vincent, Lesser Antilles. J Petrol 56:161–192
Müntener O, Ulmer P (2018) Arc crust formation and differentiation constrained by experimental petrology. Am J Sci 318:64–89
Nandedkar RH, Ulmer P, Müntener O (2014) Fractional crystallization of primitive, hydrous arc magmas: an experimental study at 0.7 GPa. Contrib Mineral Petrol 167:1–27
Paulatto M, Moorkamp M, Hautmann S, Hooft E, Morgan JV, Sparks RSJ (2019) Vertically extensive magma reservoir revealed from joint inversion and quantitative interpretation of seismic and gravity data. J Geophys Res-Sol Earth 124:11170–11191
Peate DW, Pearce JA, Hawkesworth CJ, Colley H, Edwards CMH, Hirose K (1997) Geochemical variations in Vanuatu arc lavas: the role of subducted material and a variable mantle wedge composition. J Petrol 38:1331–1358
Petford N, Atherton M (1996) Na-rich partial melts from newly underplated basaltic crust: the Cordillera Blanca Batholith, Peru. J Petrol 37:1491–1521
Petterson MG, Babbs T, Neal CR, Mahoney JJ, Saunders AD, Duncan RA, Tolia D, Magu R, Qopoto C, Mahoa H, Natogga D (1999) Geological–tectonic framework of Solomon Islands, SW Pacific: crustal accretion and growth within an intra-oceanic setting. Tectonophysics 301:35–60. https://doi.org/10.1016/S0040-1951(98)00214-5
Pichavant M, Mysen BO, Macdonald R (2002) Source and H_2O content of high-MgO magmas in island arc settings: an experimental study of a primitive calc-alkaline basalt from St. Vincent, Lesser Antilles arc. Geochim Cosmochim Acta 66:2193–2209
Plank T (2005) Constraints from thorium/lanthanum sediment recycling at subduction zones and the evolution of the continents. J Petrol 46:921–944
Putirka KD (2008) Thermometers and barometers for volcanic systems. Rev Mineral 69(1):61–120
Rasmussen DJ, Plank TA, Roman DC, Zimmer MM (2022) Magmatic water content controls the pre-eruptive depth of arc magmas. Science 375:1169–1172
Reubi O, Blundy J (2009) A dearth of intermediate melts at subduction zone volcanoes and the petrogenesis of arc andesites. Nature 461:1269–1273
Reubi O, Müntener O (2022) Making andesites and the continental crust: mind the step when wet. J Petrol 63(6):egac044. https://doi.org/10.1093/petrology/egac044
Reubi O, Nicholls IA (2005) Structure and dynamics of a silicic magmatic system associated with caldera-forming eruptions at Batur volcanic field, Bali. Indonesia J Petrol 46(7):1367–1391
Reubi O, Nicholls IA, Kamenetsky VS (2003) Early mixing and mingling in the evolution of basaltic magmas: evidence from phenocryst assemblages, Slamet Volcano, Java, Indonesia. J Volcanol Geoth Res 119(1–4):255–274
Rezeau H, Klein BZ, Jagoutz O (2021) Mixing dry and wet magmas in the lower crust of a continental arc: new petrological insights

from the Bear Valley Intrusive Suite, southern Sierra Nevada, California. Contrib Mineral Petrol 176:73. https://doi.org/10.1007/s00410-021-01832-2

Ridolfi F, Renzulli A, Puerini M (2010) Stability and chemical equilibrium of amphibole in calc-alkaline magmas: an overview, new thermobarometric formulations and application to subduction-related volcanoes. Contrib Mineral Petrol 160:45–66

Rioux M (2006) The growth and differentiation of arc crust: temporal and geochemical evolution of the accreted Talkeetna arc, south-central Alaska. Dissertation, University of California.

Rioux M, Mattinson J, Hacker B, Kelemen P, Blusztajn J, Hanghøj K, Gehrels G (2010) Intermediate to felsic middle crust in the accreted Talkeetna arc, the Alaska Peninsula and Kodiak Island, Alaska: an analogue for low-velocity middle crust in modern arcs. Tectonics 29(TC3001):2010. https://doi.org/10.1029/2009TC002541

Roedder E, Bodnar RJ (1980) Geologic pressure determinations from fluid inclusion studies. Ann Rev Earth Sci 8:263–301

Rohrbach A, Schuth S, Ballhaus C, Münker C, Matveev S, Qopoto C (2005) Petrological constraints on the origin of arc picrites, New Georgia Group, Solomon Islands. Contrib Mineral Petrol 149:685–698

Rudnick RL (1995) Making continental crust. Nature 378:571–578. https://doi.org/10.1038/378571a0

Saito S, Arima M, Nakajima T, Tani K, Miyazaki T, Senda R, Chang Q, Takahashi T, Hirahara Y, Kimura J-I (2011) Petrogenesis of the Kaitomagatake granitoid pluton in the Izu Collision zone, central Japan: implications for transformation of juvenile oceanic arc into mature continental crust. Contrib Mineral Petrol 163:611–629. https://doi.org/10.1007/s00410-011-0689-1

Schaarschmidt A, Klemd R, Regelous M, Voudouris PC, Melfos V, Haase KM (2021) The formation of shoshonitic magma and its relationship to porphyry-type mineralisation: the Maronia pluton in NE Greece. Lithos 380:105911. https://doi.org/10.1016/j.lithos.2020.105911

Schmidt MW, Jagoutz O (2017) The global systematics of primitive arc melts. Geochem, Geophys, Geosyst 18:2817–2854

Schoenhofen MV, Haase KM, Beier C, Woelki D, Regelous M (2020) Chemical evolution of calc-alkaline magmas during the ascent through continental crust: constraints from Methana, Aegean arc. J Petrol 61(3):egaa036. https://doi.org/10.1093/petrology/egaa936

Schuth S, Rohrbach A, Münker C, Ballhaus C, Garbe-Schönberg D, Qopoto C (2004) Geochemical constraints on the petrogenesis of arc picrites and basalts, New Georgia Group, Solomon Islands. Contrib Mineral Petrol 148:288–304

Schuth S, Münker C, König S, Qopoto C, Basi S, Garbe-Schönberg D, Ballhaus C (2009) Petrogenesis of lavas along the Solomon Island arc, SW Pacific: coupling of compositional variations and subduction zone geometry. J Petrol 50:781–811

Segev A, Rybakov M, Mortimer N (2012) A crustal model for Zealandia and Fiji. Geophys J Int 189:1277–1292. https://doi.org/10.1111/j.1365-246X.2012.05436.x

Sisson TW, Grove TL (1993a) Experimental investigations of the role of H_2O in calc-alkaline differentiation and subduction zone magmatism. Contrib Mineral Petrol 113:143–166

Sisson TW, Grove TL (1993b) Temperatures and H_2O contents of low-MgO high-alumina basalts. Contrib Mineral Petrol 113:167–184

Smith DJ (2014) Clinopyroxene precursors to hornblende sponge in arc crust. Nat Commun 5:1–6. https://doi.org/10.1038/ncomms5329

Smith IEM, Worthington TJ, Stewart RB, Price RC, Gamble JA (2003) Felsic volcanism in the Kermadec arc, SW Pacific: crustal recycling in an oceanic setting. In: Larter RD, Leat PT (eds) Intra-oceanic subduction systems: tectonic and magmatic processes. Geological Society, London, Special Publications, pp 99–118

Smith DJ, Petterson MG, Saunders AD, Millar IL, Jenkin GRT, Toba T, Naden J, Cook JM (2009) The petrogenesis of sodic island arc magmas at Savo volcano, Solomon Islands. Contrib Mineral Petrol 158:785–801

Sourirajan S, Kennedy GC (1962) The system H_2O-NaCl at elevated temperatures and pressures. Am J Sci 260:115–141

Spandler C, Mavrogenes J, Hermann J (2007) Experimental constraints on element mobility from subducted sediments using high-P synthetic fluid/melt inclusions. Chem Geol 239:228–249

Sun SS, McDonough WF (1989) Chemical and isotopic systematics of oceanic basalts: implications for mantle composition and processes. In: Saunders AD, Norry MJ (eds) Magmatism in the Ocean Basins. Geol Soc, London, Spec Publ 42:313–345

Suyehiro K, Takahashi N, Ariie Y, Yokoi Y, Hino R, Shinohara M, Kanazawa T, Hirata N, Tokuyama H, Taira A (1996) Continental crust, crustal underplating, and low-Q upper mantle beneath an oceanic island arc. Science 272:390–392

Suzuki K, Yamamoto S, Sawaki Y, Aoki K, Omori S, Kon Y, Hirata T, Li Y, Takaya Y, Fujinaga K, Kato Y, Maruyama S (2014) Zircon U-Pb dating from the mafic enclaves in the Tanzawa Tonalitic Pluton, Japan: implications for arc history and formation age of the lower-crust. Lithos 196–197:301–320

Suzuki K, Kitajima K, Sawaki Y, Hattori J, Hirata T, Maruyama S (2015) Ancient oceanic crust in island arc lower crust: evidence from oxygen isotopes in zircons from the Tanzawa Tonalitic Pluton. Lithos 228–229:43–54

Takagi D, Sato H, Nakagawa M (2005) Experimental study of a low-alkali tholeiite at 1–5 kbar: optimal condition for the crystallization of high-An plagiolcase in hydrous arc tholeiite. Contrib Mineral Petrol 149:527–540

Tapster S, Roberts NMW, Petterson MG, Saunders AD, Naden J (2014) From continent to intra-oceanic arc: Zircon xenocrysts record the crustal evolution of the Solomon island arc. Geology 42:1087–1090. https://doi.org/10.1130/G36033.1

Tapster S, Condon DJ, Naden J, Noble SR, Petterson MG, Roberts NMW, Saunders AD, Smith DJ (2016) Rapid thermal rejuvenation of high-crystallinity magma linked to porphyry copper deposit formation: evidence from the Koloula Porphyry Prospect, Solomon Islands. Earth Planet Sci Lett 442:206–217. https://doi.org/10.1016/j.epsl.2016.02.046

Taylor SR, McLennan SM (1985) The continental crust: its composition and evolution. Blackwell Scientific Publications, Oxford

Tsuruga K, Kasahara J, Fujii N (2006) A proposal of the active monitoring for the temporal change and spatial movement of seismic reflectors cause by magma reservoir beneath a volcano. Amer Geophys Union, Fall Meeting 2006, abstract NG42A-01.

Valley JW, Kinny PD, Schulze DJ, Spicuzza MJ (1998) Zircon megacrysts from kimberlite: oxygen isotope variability among mantle melts. Contrib Mineral Petrol 133:1–11

Whalen JB (1985) Geochemistry of an island-arc plutonic suite: the Uasilau-Yau Yau intrusive complex, New Britain, P.N.G. J Petrol 26:603–632

Woelki D, Haase KM, Schoenhofen MV, Beier C, Regelous M, Krumm SH, Günther T (2018) Evidence for melting of subducting carbonate-rich sediments in the western Aegean arc. Chem Geol 483:463–473. https://doi.org/10.1016/j.chemgeo.2018.03.014

Workman RK, Hart SR (2005) Major and trace composition of the depleted MORB mantle (DMM). Earth Planet Sci Lett 231:53–72

Yukutake Y, Abe Y, Honda R, Sakai S (2021) Magma reservoir and magmatic feeding system beneath Hakone volcano, central Japan, revealed by highly resolved velocity structure. J Geophys Res-Sol Earth 126(4):e2020JB021236. https://doi.org/10.1029/2020JB021236